Entropy Balance, Multibaker Maps, and the Dynamics of the Lorentz Gas

T. Tél and J. Vollmer

Contents

§1. Introduction 369
§2. Coarse Graining and Entropy Production in Dynamical Systems . . . 371
2.1 Exact and Coarse-Grained Densities 371
2.2 Gibbs and Coarse-Grained Entropies 373
2.3 Irreversible Entropy Production 376
2.4 Entropy Balance 377
2.5 Entropy Balance for Steady States 377
2.6 Closed Volume-Preserving Systems 378
2.7 Missing Ingredients to a Thermodynamic Description 379
§3. From the Lorentz Gas to Multibaker Maps 380
3.1 Mapping Relating Subsequent Scattering Events for an Unbiased Dynamics with Periodic Boundary Conditions . 381
3.2 Adding an External Field and a Reversible Thermostat 384
3.3 The Spatially-Extended Lorentz Gas 386
3.4 Symbolic Dynamics and Pruning 389
3.5 Piecewise-Linear Approximation of the Lorentz Dynamics . . . 390
3.6 The Next-To-Nearest-Neighbor (nnn) Multibaker Map 390
§4. Transport and Entropy Production in the (nnn) Multibaker Map . . . 394
4.1 Time Evolution of the Entropies 395
4.2 The Macroscopic Limit for Transport and the Advection-Diffusion Equation 396
4.3 The Macroscopic Limit for the Entropy Balance 397
4.4 Entropy Production in the Macroscopic Limit 398
§5. Results Obtained with (nn) Multibaker Maps 400
5.1 Invariant Densities and Takagi Functions 400
5.2 Particle Transport and Entropy Balance in Isothermal Systems 402

5.3 Green-Kubo Relation in the Isothermal Case 403
5.4 Energy Transport 404
5.5 The Entropy Balance in the Presence of Temperature Gradients 405
5.6 Thermoelectric Cross Effects 406
5.7 The Irreversible Entropy Production as the Average Growth Rate of the Relative Phase-Space Density in Steady States . . . 408
5.8 Fluctuation Theorem for Entropy Production in Steady States with Density Gradients 409
§6. Discussion 411
6.1 Deviations from Dynamical Systems Theory 411
6.2 Interpretation of Coarse Graining 412
6.3 Interpretation of the Macroscopic Limit 413
6.4 Outlook and Open Problems 414
Appendix 414
A. Trajectories of the Thermostated Lorentz Gas 414
A.1 Time Reversibility and Phase-Space Contraction 415
A.2 The Form of Trajectories 415
References 416

Abstract. We extend and review recent results on nonequilibrium transport processes described by multibaker maps. The relation of these maps to the dynamics of the Lorentz gas is discussed. Special emphasis is put on the concept of coarse graining and its use in defining the analog of thermodynamic entropy and in deriving an entropy balance. A full analogy with Irreversible Thermodynamics can only be obtained if at certain points we deviate from traditional dynamical system theory, and allow for open boundary conditions which make the system to converge to a 'forced' stationary measure. This measure differs from the natural SRB measure which can be realized with periodic boundary conditions only.

§1. Introduction

Entropy production is a measure of deviation from thermal equilibrium [1–6]. It is a surprising result of the last years that a consistent definition of this central concept of Irreversible Thermodynamics can be given for general dynamical systems. For closed systems with periodic boundary conditions, the description of the effect of an applied external field and of a reversible thermostating mechanism has been pioneered by Hoover and Evans and their respective coworkers [3]. A rigorous treatment of the same problem was first suggested by Chernov et al [7], and was further worked out by Ruelle [8]. These approaches model the transport process by dissipative dynamical systems and relate the transport coefficients and other physical observables to properties of the invariant SRB measure. A concept of steady-state entropy production in dynamical systems has been based on the average phase-space contraction rate [3, 9, 10]. In an alternative approach, open volume preserving dynamics are considered subjected to absorbing boundary conditions. In such cases the escape rate from the non-attracting invariant set responsible for transient chaos is related to the transport coefficients [11–14], and to the entropy production [15].

The heart of Irreversible Thermodynamics [2] is to set up an entropy balance for the thermodynamic entropy S. This balance is commonly written in the form

$$\frac{dS(t)}{d\,t} = \frac{d_e S(t)}{d\,t} + \frac{d_i S(t)}{d\,t}. \tag{1}$$

Its right hand side contains the sum of the external and internal changes of entropy, i.e., changes due to an entropy flux out of the considered volume and due to irreversible entropy production. The latter is non-negative, while the former one can have any sign. For noisy dynamics this entropy balance was derived by Nicolis and Daems [16] for the Gibbs entropy of systems subjected to (arbitrary) small noise. In the present paper, we show – by extending the results of [15] – that such a relation can also be found in *deterministic* systems if a suitably chosen *coarse-grained entropy* is considered. Statements about general dynamical systems unavoidably refer to global properties, i.e., they contain the full system's entropy, and cannot provide a comprehensive thermodynamic description of transport driven by spatial inhomogeneities of the thermodynamic variables. To this end *local* relations are needed.

Multibaker maps have been introduced to model transport in open systems, *i.e.*, systems where transport can be induced by suitably chosen boundary conditions. In the original model of Gaspard [17–20] the dynamics is fully Hamiltonian and describes a diffusion process compatible with Fick's law. Later it was extended to model chemical reactions, too [21]. The invariant measure belonging to these problems is not the Liouvillian, but a fractal distribution *forced* on the system by different densities prescribed at the two ends. The irreversible entropy production is due to a kind of mixing entropy, which can only be understood by using the concept of coarse graining. Multibaker models

can also describe transport driven by boundary conditions *and* external fields [22–33]. The latter driving typically requires a thermostating mechanism, and due to this, a deviation from local phase-space volume preservation. The irreversible entropy production then contains contributions from both the average phase-space contraction rate and the mixing entropy. Early versions of this class of models describe particle transport by the traditional piecewise-linear map [22–25]. Later on the changes due to a nonlinear form were worked out [26], and the linear version was used to derive fluctuation relations [27]. The most recent versions have been extended to deal with simultaneous particle and heat transport [28–32].

One of the appealing features of this approach is that it permits a comparison with a local thermodynamic entropy balance

$$\partial_t s = \Phi + \sigma^{(\mathrm{irr})}. \tag{2}$$

Here s is the entropy density, and Φ and $\sigma^{(\mathrm{irr})}$ represent the entropy flux density and the rate of irreversible entropy production per unit volume, respectively. For systems with gradients of the thermodynamic fields, multibakers are up to now the only models for which a consistency with the local entropy balance could be found.

Some authors (e.g., [33], and Dettmann in this volume) consider multibaker maps as abstract models of little physical relevance. In contrast, we show here that they mimic the evolution of independent particles in the Lorentz gas driven by an external field and subjected to nonequilibrium boundary conditions. They form the only analytically accessible class of systems that allows us to find constraints on the dynamics needed to achieve a consistent description of the entropy balance, and of the transport equations and transport coefficients.

We first discuss how far one can go towards an entropy balance in a classical dynamical system (Sect. 2), and in later sections we describe which additional features have to be imposed on the dynamics to permit a consistent thermodynamic description. In Sect. 3 we show how, via a sequence of transformations and approximations, one can 'derive' a five-strip multibaker map mimicking the dynamics of independent particles in the driven Lorentz gas. The required particle trajectories of the Lorentz gas are given in the Appendix. The entropy production for the resulting multibaker map is derived in Sect. 4. In Sect. 5 results found with the earlier studied three-strip multibaker model are summarized. The paper is concluded in Sect. 6 by a discussion and outlook.

§2. Coarse Graining and Entropy Production in Dynamical Systems

We treat *invertible* and *hyperbolic* [34, 35] dynamical systems whose phase space[1] is either closed or open. In the former case we consider the full phase space (accessible to the particles in the presence of some general constraints). In the latter, we restrict our attention to a fixed finite phase-space volume of interest corresponding to the motion in a finite region of the configuration space. Particles can escape this volume with some escape rate κ [36]. In both cases the dimension of the phase space is denoted by d.

On general grounds, one expects that closed Hamiltonian systems can only be used as models of thermal equilibrium, or fluctuations around it (cf. Sec. 2.6). Models for nonequilibrium processes based on low-dimensional dynamical system must therefore either be dissipative [3] or, if phase-space-volume preserving, their phase space has to be open. The long-time dynamics is then associated with either an SRB measure on a chaotic attractor [34, 35] or with a conditionally invariant measure [36–38] located on the invariant manifolds of the open volume-preserving system. (For simplicity we call both measures natural.) As a consequence, the nonequilibrium processes are associated with *fractal* phase-space structures, which have no volume with respect to the Liouville measure. The set of average Lyapunov exponents characterizing the related invariant set will be denoted by $\bar{\lambda}_1 \geq \bar{\lambda}_2 \geq \cdots \bar{\lambda}_d$, and the location dependent eigenvalues of the linearized dynamics are accordingly $\lambda_1 \geq \lambda_2 \geq \cdots \lambda_d$.

The key observation in trying to model irreversible processes by dynamical systems is the ever refining phase-space structures associated with the convergence towards the fractal measure. It is impossible to describe the asymptotic states by smooth stationary densities in phase space. Instead, we suggest to consider a *coarse-grained* description which is interpreted as an approach where the ever refining structures in phase space are followed with a finite resolution. Comparing the time evolution in this coarse-grained description with the exact one, gives new insight in the dynamics and into the possible structure of a macroscopic description of transport. For illustrational purposes, we confine ourselves to discuss only the simplest possible coarse graining, which consists in dividing the adimensionalized phase space into identical boxes of linear size ε much smaller than unity ($\varepsilon \ll 1$). The phase-space volume of the boxes is then ε^d.

2.1 Exact and Coarse-Grained Densities. We use two different phase-space densities belonging to the same smooth initial condition

- $\varrho(\mathbf{x}, t)$, the *exact phase-space density* at phase-space location $\mathbf{x}$ and time t, and

[1] By phase space we mean here the phase space of a dynamical system without yet the structures required to set up statistical mechanics.

- $\varrho_\varepsilon(i,t)$, the *coarse-grained density* of box i at time t, which is obtained by averaging $\varrho(\mathbf{x},t)$ over box i.

The averaging on the set of boxes defines the coarse graining. (For simplicity we use the same notations for the conditionally invariant density and its coarse-grained version characterizing open systems. Both types of densities are normalized to unity.)

After long times there is a qualitative difference between the exact and the coarse-grained densities: the exact density keeps developing finer and finer structures and has no time-independent limit. It becomes undefined as a density and its asymptotic distribution is to be described by the natural invariant measure μ [34, 35]. On the other hand, the coarse-grained density converges to a (piecewise constant) *stationary distribution* $\bar{\varrho}_\varepsilon(i)$ such that the natural measure $\mu_i(\varepsilon)$ of box i equals $\bar{\varrho}_\varepsilon(i)\varepsilon^d$. The asymptotic temporal dependence of $\varrho(\mathbf{x},t)$ can be written as

$$\varrho(\mathbf{x},t) \sim e^{\sigma(\mathbf{x})t}, \tag{3}$$

while

$$\varrho_\varepsilon(i,t) \sim \bar{\varrho}_\varepsilon(i). \tag{4}$$

Here $\sigma(\mathbf{x})$ is the local phase-space contraction rate [3, 5] at point $\mathbf{x}$. Equation (3) follows from the fact that the phase-space volume around $\mathbf{x}$ is behaving like $\exp[-\sigma(\mathbf{x})t]$ and the measure of a given volume is not changing in time due to the conservation of probability. In closed systems the phase-space contraction rate is the negative sum of all the local eigenvalues [3]

$$\sigma(\mathbf{x}) = -\sum_{j=1}^{d} \lambda_j(\mathbf{x}), \tag{5a}$$

in open volume-preserving systems this role is played by the escape rate [15]

$$\sigma(\mathbf{x}) = \kappa. \tag{5b}$$

This last equation expresses the fact that the effective volume in a fixed portion of the phase space is decreasing due to escape, in spite of the preservation of volume in the full phase space. The escape rate is an effective phase-space contraction rate for open systems. The state in which the coarse grained density is stationary we call a *steady state*.

The qualitative difference between the behavior of the exact and the coarse-grained densities [cf. (3), (4)] is a *hallmark of irreversibility*: every macroscopic description of transport is based on coarse-grained densities and hence does not resolve *all* information on the fine details of the system's phase-space dynamics.

How quickly the two densities differ depends on the type of initial conditions.

A. For extended initial density profiles, the difference is in the beginning on the order of the box size ε and is negligible. Strong deviations start to develop only after a crossover time t_ε set by the fact that the support of the density in the stable directions becomes of the same order as the box size, due to the contraction with the negative Lyapunov exponents. An upper limit to this time scale is

$$t_\varepsilon \approx -\frac{1}{\bar{\lambda}_-} \ln \varepsilon. \tag{6}$$

where $\bar{\lambda}_-$ is the largest amongst the negative average Lyapunov exponent (the smallest one in modulus). In typical dynamical systems this Lyapunov exponent is of order unity. Thus, the crossover time is also on the order of unity, and depends logarithmically on the box size.

B. When the initial condition is sharply localized, concentrated in a single box only, so that $\varrho(x,0) = \varepsilon^{-d}$, the strong deviation is immediate since the coarse-grained density does not feel any contraction in the stable directions. The change of the phase-space volume is due to the expanding directions and the volume starts to grow in time as $\exp(kt)$, where $k = \sum_{\lambda_j>0} \lambda_j$ is the sum of the positive local eigenvalues $\lambda_j > 0$. Open systems soon start to feel the effect of escape leading to a crossover of the growth rate towards $k = \sum_{\lambda_j>0} \lambda_j - \kappa$, i.e., the difference of the sum of positive local eigenvalues and the escape rate. Therefore, initially the coarse-grained density behaves in all occupied boxes approximately as

$$\varrho_\varepsilon(i,t) \approx \varepsilon^{-d} \exp(-kt). \tag{7}$$

Due to Pesin's theorem [35] and its generalization for escaping systems [38–40] the metric (or Kolmogorov-Sinai) entropy h_{KS} for the motion on the invariant set is $h_{KS} = \sum_{\bar{\lambda}_j>0} \bar{\lambda}_j - \kappa$. For very localized initial conditions the average value of k is thus the metric entropy $\bar{k} = h_{KS}$. The coarse-grained density typically starts to grow exponentially with the metric entropy as its rate.

2.2 Gibbs and Coarse-Grained Entropies. A natural choice for the entropy characterizing the state of the system at time t is the information-theoretic entropy taken with respect to a phase-space density at that time. Since we simultaneously consider the time evolution of the exact and the coarse-grained densities, two entropies are defined:

- The entropy $S^{(G)}$ is evaluated with respect to the exact density:

$$S^{(G)}(t) \equiv -\int \mathrm{d}^d x \; \varrho(\mathbf{x},t) \ln\left(\frac{\varrho(\mathbf{x},t)}{\varrho^*}\right), \tag{8}$$

where ϱ^* is a constant reference density. $S^{(G)}$ is commonly referred to as the *Gibbs entropy*.

- The *coarse-grained entropy* S_ε is defined in an analogous way as a sum over boxes of size ε

$$S_\varepsilon(t) \equiv -\sum_i \varrho_\varepsilon(i,t)\, \varepsilon^d\, \ln\left(\frac{\varrho_\varepsilon(i,t)}{\varrho^*}\right), \tag{9}$$

where the notation expresses that the coarse-grained entropy depends on the box size ε.

The time evolution of the entropies immediately follows from that of the densities.

A. For extended initial conditions, $S^{(G)}$ and S_ε nearly coincide before the crossover time t_ε is reached. Typically they both decrease since the distributions start approaching the one on the invariant set and hence the information content is increasing. This tendency does not change for $S^{(G)}$ which keeps decreasing after t_ε. In view of (8) and (3) we find:

$$S^{(G)}(t) = -\sigma(t)t + \text{const}, \tag{10}$$

where $\sigma(t)$ is the average of the phase-space contraction rate (5) evaluated with respect to $\varrho(x,t)$ at time t. The asymptotic behavior is a linear decay

$$S^{(G)}(t) \to -\bar{\sigma}t \tag{11}$$

with $\bar{\sigma}$ as the long-time average of phase-space contraction rate taken with respect to the natural measure. The coarse-grained entropy, on the other hand, goes into saturation since with the given resolution the localization of the invariant set does not change any longer after t_ε. Asymptotically, the coarse-grained entropy tends to a constant $\bar{S}_\varepsilon$ which depends on the box size but is *independent* of the initial condition:

$$S_\varepsilon(t) \to \bar{S}_\varepsilon. \tag{12}$$

This expresses the convergence of the coarse-grained density to a stationary value. In contrast to $S^{(G)}$, the coarse-grained entropy has a *dissipative* dynamics with a *fixed point attractor*.

B. For sharply localized initial conditions localized to a single box, both S and $S^{(G)}$ are initially $\ln(\varrho^*\varepsilon^d)$ and start increasing because the distribution is spreading out. Since the coarse-grained density behaves according to (7), its initial growth is described by

$$S_\varepsilon(t) = \ln(\varrho^\star\, \varepsilon^{-d}) + kt \approx S_\varepsilon(t=0) + h_{KS}\, t. \tag{13}$$

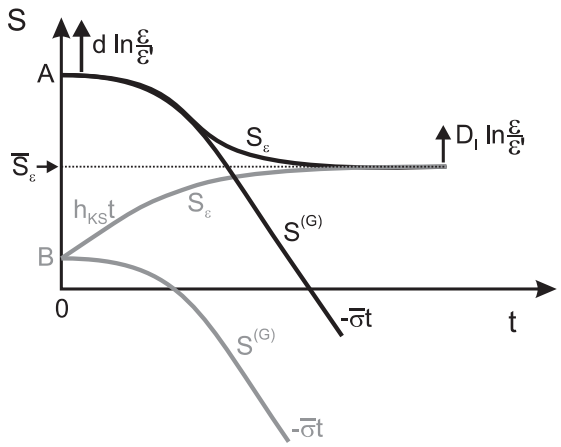

Figure 1: Time evolution of the entropies in dissipative or open volume preserving dynamical systems relaxing towards a steady state. The black and gray lines/symbols correspond to the respective initial conditions A and B described in the text. The arrows represent the shift of the coarse-grained entropy curves, when decreasing the resolution from ε to $\varepsilon' < \varepsilon$.

Later the coarse-grained entropy approaches exactly the same limit (12) as in the case of extended initial conditions. The growth of the Gibbs entropy deviates from the linear law since the support of the exact density also feels the contraction towards the unstable foliation. Due to this effect, it starts decreasing and asymptotically it shows the same linear decay (11) as with extended initial conditions, just shifted downwards (Fig. 1).

In the following subsection we discuss in detail the strong temporal difference in the dynamics of these two entropies, and how the rate of irreversible entropy production can be related to this observation.

Before, however, it is worth briefly discussing the dependence of the entropy on the resolution ε. To this end, we assume (cf. [41]) that the reference density is ε-dependent according to the law

$$\varrho^* = \bar{\varrho}^* \varepsilon^{-d}. \tag{14}$$

The ε-dependence of the asymptotic coarse-grained entropy can then be expressed by a number: the information dimension D_I of the coarse-grained steady-state distribution, i.e., of the natural invariant measure μ. This quantity has been introduced in the context of the multifractal characterization of the natural measures of chaotic attractors and of other fractal distributions [42–44]. For every stationary measure characterized by boxes of very small (but finite) linear size ε, which carry probabilities $p_i(\varepsilon)$, the information dimension is defined

via the asymptotic relation $-\sum_i p_i(\varepsilon) \ln p_i(\varepsilon) \sim -D_I \ln \varepsilon$. In view of this, the dependence of $\bar{S}_\varepsilon$ on ε for fine enough resolutions is

$$\bar{S}_\varepsilon = -D_I \ln \varepsilon \tag{15}$$

where $D_I < d$ is the information dimension of the natural measure. If we refine the box size from ε to $\varepsilon' < \varepsilon$, the saturation value is shifted upward by $D_I \ln(\varepsilon/\varepsilon')$ (Fig. 1). At the same time the initial value of the entropy characterizing the initial condition is also shifted upward but by an amount of $d \ln(\varepsilon/\varepsilon')$. After all, the information dimension of smooth measures is the dimension of the phase space. This implies that for a higher resolution (smaller ε) the steady-state distribution will be reached at later times, as already stated by Eq. (6). It is interesting to note that besides the actual time evolution of the Gibbs and the coarse-grained entropies, two traditional, entropy-derivative type quantities, which are well-known in dynamical system theory, also appear in Fig. 1. The metric entropy h_{KS} is the temporal derivative of the information theoretic entropy taken with respect to the symbol-sequence distribution in a symbolic encoding [35] (cf. Sect. 3.4 below for an example of a the symbolic encoding), and D_I is the $\ln(1/\varepsilon)$ derivative of the information theoretic entropy taken with respect to the box probabilities.

2.3 Irreversible Entropy Production. The difference between the coarse-grained and the Gibbs entropy characterizes the information on the exact state of the system which cannot be resolved in the coarse-grained description. The temporal change of this quantity measures thus the rate of the loss of information on the exact state of the system. In view of this, we suggest (see also [22–24]) to identify this temporal change at any instant of time with the *rate of irreversible entropy production* $\Sigma_\varepsilon^{(irr)}$ of the dynamical system,

$$\Sigma_\varepsilon^{(irr)}(t) \equiv \frac{d}{d\,t} \left(S_\varepsilon(t) - S^{(G)}(t) \right). \tag{16}$$

It is defined for every dynamical system, and for sufficiently large t it is typically non-negative (cf. Fig. 1)

$$\Sigma_\varepsilon^{(irr)}(t) \geq 0 \tag{17}$$

in accordance with the analogous thermodynamic quantity. Note that in spite of the ε-dependence of the coarse-grained entropy, the entropy production depends only slightly on the coarse graining. Latest upon reaching the steady state where the coarse grained density and S_ε become time-independent, the ε-dependence fully disappears from the entropy production: $\Sigma_\varepsilon^{(irr)}(t) \to \bar{\Sigma}^{(irr)}$.

The difference in slopes between the coarse-grained and the Gibbs entropy becomes pronounced after the crossover time t_ε, leading to a substantial entropy production for $t > t_\varepsilon$. This clearly shows that we are lacking information on the exact asymptotic state when applying a description with a finite resolution.

2.4 Entropy Balance. Interestingly, a decomposition of the time derivative of the coarse-grained entropy, very similar to Eq. (1), can be given for general dynamical systems by taking the time derivative of the identity $S_\varepsilon = S^{(G)} + (S_\varepsilon - S^{(G)})$:

$$\frac{dS_\varepsilon(t)}{d\,t} \equiv \Phi(t) + \Sigma_\varepsilon^{(irr)}(t), \tag{18}$$

and interpreting

$$\Phi(t) \equiv \frac{dS^{(G)}(t)}{d\,t} \tag{19}$$

as an entropy flux through the system which does not cause irreversible changes. Note that this is defined as the change of the Gibbs entropy. From (10) we deduce that

$$\Phi(t) = -\sigma(t) - t\,\frac{d\,\sigma(t)}{d\,t} \approx -\sigma(t), \tag{20}$$

where in the last step we used the approximation that the time derivative of the average phase-space contraction rate tends to zero much faster than $1/t$. Eq. (20) directly relates the entropy flux to the average phase-space contraction rate at any instant of time. Note that it is *independent* of ε.

The definitions of $\Sigma_\varepsilon^{(irr)}$ and Φ show that it is impossible to find an entropy balance by *merely* considering the Gibbs entropy. An analogy with thermodynamics can only be obtained by simultaneously following the exact time evolution characterized by the Gibbs entropy and comparing it to a coarse-grained description.

2.5 Entropy Balance for Steady States. From (10), (12) and (16) we find for the stationary entropy production $\bar{\Sigma}^{(irr)}$ that

$$\bar{\Sigma}^{(irr)} \equiv \Sigma^{(irr)}(t \to \infty) = \bar{\sigma} > 0 \tag{21}$$

irrespective of the box size. For every dynamical system [8, 15] the rate of irreversible entropy production in a steady state is the average phase-space contraction rate.

Since in steady states the coarse-grained entropy is constant, the flux indeed compensates entropy production and

$$\bar{\Phi} \equiv \frac{d}{d\,t} S^{(G)}(t) \to -\bar{\sigma}. \tag{22}$$

This formula explains the result obtained via heuristic arguments by several authors [3, 5, 7, 8] stating that the derivative of the Gibbs entropy is the negative of the average phase-space contraction rate in a steady state, and hence

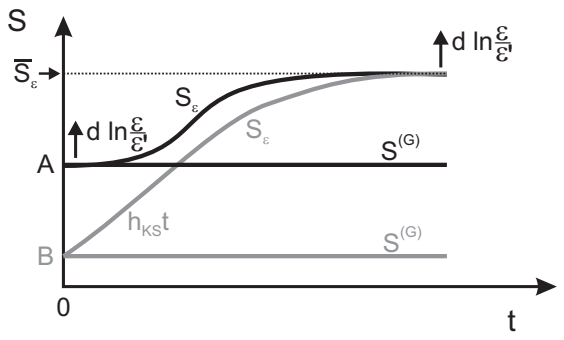

Figure 2: Time evolution of the entropies in a closed volume-preserving dynamical system relaxing towards an equilibrium state. The black and gray lines/symbols correspond to the respective initial conditions A and B described in the text. The arrows represent the shift of the coarse-grained entropy curves when decreasing the resolution from ε to $\varepsilon' < \varepsilon$.

of the steady-state entropy production. Note that this is not a property of thermodynamics but of dynamical-systems theory.

Using again that $h_{KS} = \sum_{\bar{\lambda}_j>0} \bar{\lambda}_j - \kappa$ for general open systems, we obtain

$$\bar{\Phi}^{(irr)} = \sum_{\bar{\lambda}_i<0} \bar{\lambda}_i + h_{KS}. \tag{23}$$

Thus, in a steady state we find a relation between the entropy flux and the metric entropy. The first term is negative and expresses the decrease of the entropy due to the convergence towards the invariant set, the second one represents the increase due the chaoticity of the dynamics.

It is interesting to see that in two-dimensional chaotic maps the irreversible entropy production essentially determines the information dimension of the natural measure. Since in general $D_I = 1 + (\kappa - \bar{\lambda}_1)/\bar{\lambda}_2$ [38], we find [15] that

$$D_I = 2 + \frac{\bar{\Sigma}^{(irr)}}{\bar{\lambda}_2}. \tag{24}$$

The deviation of the natural measure's dimension from the phase-space dimension ($d = 2$) is thus proportional to the irreversible entropy production in the steady state. This is valid for both closed dissipative and open volume-preserving systems.

2.6 Closed Volume-Preserving Systems. According to the above considerations, a vanishing irreversible entropy production in a steady state is only consistent with a volume-preserving dynamics (for instance, the Hamiltonian equations of motion in classical mechanics). To see how the vanishing of the

entropy production comes about in the steady state of such a system, we briefly consider the evolution of the Gibbs and the coarse-grained entropies again. The basic difference to the cases considered above is that the Gibbs entropy cannot change in time due to Liouville's theorem, *i.e.*, due to $\sigma(x) \equiv 0$ (see also [45]). The time evolution of the coarse-grained entropy depends again on the initial conditions.

A. With extended (spatially non-constant) initial conditions the coarse-grained entropy first slightly changes but after t_ε it increases and eventually saturates at a constant according to (12) (Fig. 2).

B. For a sharply localized initial condition the coarse-grained entropy starts to increase linearly as $h_{KS}t$ and approaches asymptotically the same $\bar{S}_\varepsilon$ as with the other initial conditions.

Entropy is produced only until reaching the steady state, where $\bar{\Sigma}^{(irr)} = 0$. By increasing the resolution, both the non-zero initial value and the asymptotic value is shifted by $d \ln (\varepsilon/\varepsilon')$, in accordance with the fact that $D_I = d$. After all, the asymptotic distribution is homogeneously space filling.

We conclude that the same approach of following the exact and the coarse-grained densities that we used in the presence of asymptotic fractal structures in the phase space of open and/or dissipative systems, also describes the relaxation towards a uniform density in closed, volume-preserving systems. Similarly to the difference in the behavior of systems approaching thermal equilibrium and nonequilibrium steady states, the temporal change of the entropies is markedly different in these cases (cf. Figs. 1 and 2).

2.7 Missing Ingredients to a Thermodynamic Description. The entropy production and entropy balance derived above are valid for every dynamical system. The balance equation already has the structure well-known in thermodynamics, but more than this cannot be achieved in such generality. A full agreement with thermodynamics would require in addition that Φ and $\Sigma_\varepsilon^{(irr)}$ can be expressed by coarse-grained currents. In particular, the entropy flux, which is based on the exact phase-space density and on the Gibbs entropy should be related to the divergence of a coarse-grained entropy current.

An important condition to pursue such a further comparison is the existence of coordinates representing the (macroscopic) spatial extension of the system and the focus on (macroscopically) large observation times. The up to now most commonly used approach of this type is that of dissipative (thermostated) dynamical systems with periodic boundary conditions [3, 9, 46–56]. Periodicity mimics a large spatial extension. In the steady state an agreement with the thermodynamic entropy production is then obtained in the sense of (22), even without explicitly referring to coarse graining. However, this approach is by construction unable to deal with boundary conditions ensuring sustained density gradients in the system. Moreover, one cannot address local relations since characteristics of dynamical systems are global in nature.

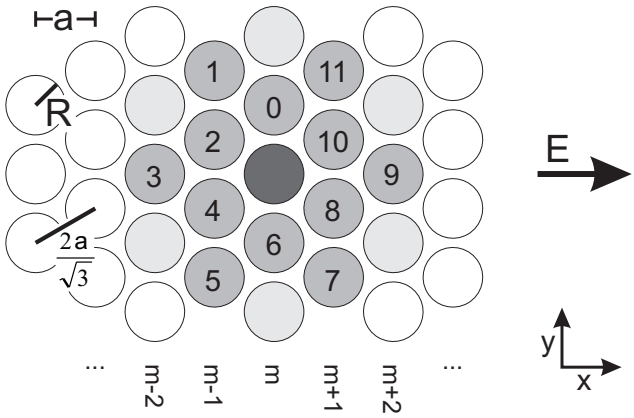

Figure 3: Arrangement of the scatters on a triangular lattice; a denotes the lattice spacing and R the radius of scatterers. The distance between neighboring disks is $2a/\sqrt{3}$. Subsequent columns of scatterers are labeled by the index m. We will allow for an external field E parallel to the x axis. The numbers $0, \cdots, 11$ inside the scatterers denote the values of the symbols s of those disks which can be hit immediately after leaving the one in the center. For $E \neq 0$, in addition to these also the light shaded disks can be reached.

In the framework of multibaker maps [17, 22] flux and absorbing boundary conditions can be implemented, and the time evolution of coarse-grained and exact densities can be followed. Agreement with local thermodynamic relations can be achieved in a suitably chosen *macroscopic limit*, which comprises the limit of large linear size and long observation times [13]. It turns out then that the weak resolution-dependence of the entropy production and of the time derivative of the coarse-grained entropy, which are present in general dynamical systems, can *disappear* in this limit, leading to a full consistency with thermodynamics [24]. On the other hand, in this class of models the agreement is only achieved on expense of *deviations* from dynamical system theory in certain points, as will be discussed later.

§3. From the Lorentz Gas to Multibaker Maps

The above considerations concerning the relation between thermodynamic properties and an underlying chaotic dynamics can conveniently be explored by studying diffusion of independent particles scattering elastically from a periodic array of circular scatterers (Fig. 3). To avoid technical difficulties arising from trajectories which travel infinitely far between collisions (*i.e.*, an array of scatters with an *infinite horizon*), we choose a triangular arrangement of scatterers and

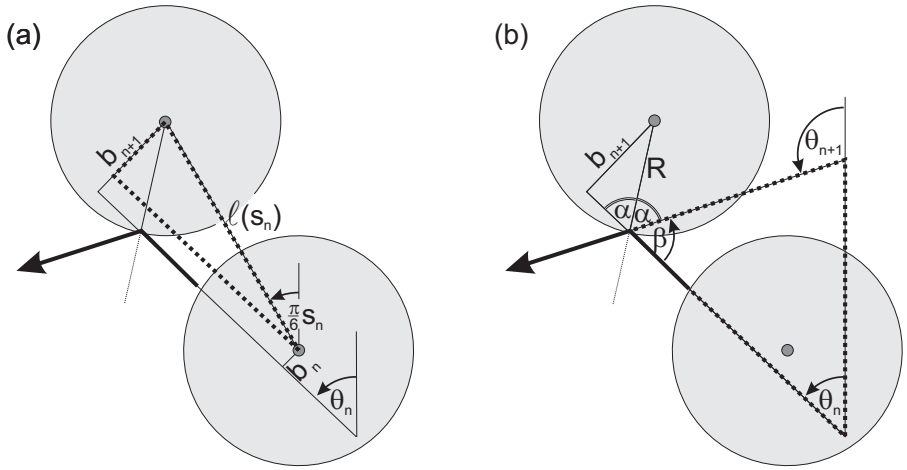

Figure 4: Definition of the impact parameter b_n and the direction of the trajectory θ_n, as well as their respective images (b_{n+1}, θ_{n+1}) for a collision with the scatterer encoded by s_n relative to the disk of the nth collision. (a) The dependence of b_{n+1} on b_n and θ_n, and (b) the one of θ_{n+1} on b_{n+1} and θ_n. The centers of the scatterers are indicated by grey bullets; all other symbols are explained in the text. Note that b_n and b_{n+1} are negative here for our convention for the sign of the impact parameter.

fix the lattice spacing a to be twice the radius of the scatterers $R = a/2$, *i.e.*, we fix a to the largest value where the horizon is finite. We set the mass and the charge of the particles to unity. The momentum vector $\mathbf{p}$ of the particles does not change its modulus upon collision.

3.1 Mapping Relating Subsequent Scattering Events for an Unbiased Dynamics with Periodic Boundary Conditions. In the field free case, the trajectories proceed along straight lines segments between subsequent scattering events. Each of these segments is uniquely characterized by two real numbers. The continuous time evolution can therefore be reduced to a mapping $\mathcal{M}$ from any of these pairs to the next one. A convenient form of the mapping is found by choosing these numbers as the angle θ of the trajectory with the y axis, and as the impact parameter $b \equiv (R_x p_y - R_y p_x)/R$ (cf. Fig. 4). Here, (R_x, R_y) denotes the vector from the center of the disk to the location of impact on its circumference. We specify the scatterer hit in collision $n+1$ (cf. Fig. 3) by $s_n = 0, \cdots, 11$, and introduce $l(s_n)$ for the distance of this scatterer and the scatterer hit at collision n. The latter takes the value $2a/\sqrt{3}$ and $2a$ for even and odd values of s_n, respectively. From the marked triangle in Fig. 4a one verifies that $\sin\left(\theta_n - \frac{\pi}{6} s_n\right) = -(b_{n+1} - b_n)/l(s_n)$. Moreover, by observing in Fig. 4b that $\sin\alpha = -b_{n+1}/R$ and $\beta = \pi - 2\alpha$, and using that the angles of the dashed triangle add up to π, one immediately determines θ_{n+1}.

This leads to

$$\mathcal{M}:\begin{pmatrix} b_n \\ \theta_n \end{pmatrix} \mapsto \begin{pmatrix} b_{n+1} \\ \theta_{n+1} \end{pmatrix} \equiv \begin{pmatrix} b_n - l(s_n)\,\sin\left(\theta_n - \frac{\pi}{6}s_n\right) \\ \theta_n + \pi + 2\arcsin\left(\frac{b_{n+1}}{R}\right) \end{pmatrix}. \tag{25}$$

By definition $b \in [-R, R]$ and θ can be taken in $[0, 2\pi]$ such that $\mathcal{M}$ is defined on the *fundamental domain* $[-R, R] \times [0, 2\pi]$. The symbol $s_n = 0, \cdots, 11$ labels *different branches* of the mapping. They are separated by the lines (Fig. 5a)

$$b = \tfrac{4R}{\sqrt{3}}\sin\left(\theta - \tfrac{\pi}{6}s\right) \pm R \quad s \in \{0, 2, 4, 6, 8, 10\}\ , \tag{26}$$

where the impact parameter takes one of its extreme values $b = \pm R$ in the next collision, *i.e.*, where the trajectories become tangent to the scatterers. Up to a trivial shift in the angle θ the action of the mapping is the same on all branches carrying an odd (even) label s. A straightforward calculation shows that $\mathcal{M}$ bijectively maps the fundamental domain onto itself (Fig. 5). Moreover, the dynamics locally preserves the area of volume elements such that an initially uniform density stays uniform at all times.[2] Since the Lorentz gas has a mixing dynamics (cf. [34, 57] for details) every smooth initial density will asymptotically approach this uniform density.

The motion of a particle in the field free Lorentz gas can be traced backward by inverting its velocity at any given time. At a collision this corresponds to the action $b_{n+1} \mapsto -b_{n+1}$ and $\theta_{n+1} \mapsto \pi + \theta_n$ which leads to the involution

$$\mathcal{T}:\begin{pmatrix} b \\ \theta \end{pmatrix} \mapsto \begin{pmatrix} -b \\ \theta - 2\arcsin(b) \end{pmatrix} \tag{28}$$

as a time-reversal operator of $\mathcal{M}$. Indeed, by straight forward calculations one verifies that

$$\mathcal{T}\mathcal{T} = 1, \tag{30}$$

$$\mathcal{M}^{-1} = \mathcal{T}\mathcal{M}\mathcal{T}. \tag{31}$$

By this mapping time reversibility is thus connected to a pairwise interchanging of possible initial conditions, *i.e.*, to a geometrical operation on points in the fundamental domain. We stress that $\mathcal{T}$ is area preserving. The determinant of its Jacobi matrix identically takes the value -1.

---

[2] This can be checked by verifying that the Jacobi matrix M_J of the mapping (25) takes the form

$$M_J = \begin{pmatrix} 1 & -l(s_n)\cos(\theta_n - \pi s_n/6) \\ 2[R^2 - b_{n+1}^2]^{-1/2} & 1 - 2l(s_n)\cos(\theta_n - \pi s_n/6)[R^2 - b_{n+1}^2]^{-1/2} \end{pmatrix}, \tag{27}$$

which has unit determinant irrespective of the values of b_{n+1} and θ_n. A graphical illustration is given in Fig. 7a.

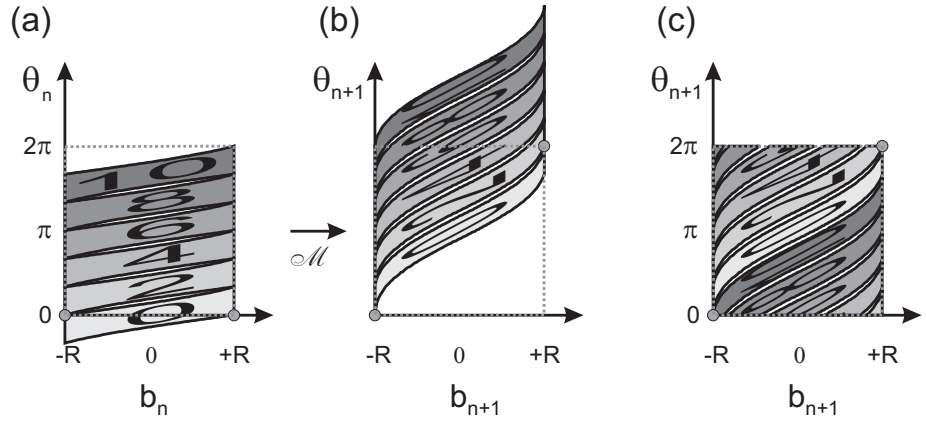

Figure 5: Graphical illustration of the action of the mapping $\mathcal{M}$ (25). (a) Location of the branches. The ones with odd numbers are not labeled. (b) Images of the respective branches. (c) Images in the fundamental domain $(b, \theta) \in [-R, R] \times [0, 2\pi]$, as obtained by using the 2π periodicity of θ_{n+1}.

The mapping $\mathcal{M}$ is a composition $\mathcal{M} = \mathcal{M}_2 \circ \mathcal{M}_1$ of the operations $\mathcal{M}_1$ and $\mathcal{M}_2$. The first one

$$\mathcal{M}_1 : \begin{pmatrix} b \\ \theta \end{pmatrix} \mapsto \begin{pmatrix} b - l(s) \ \sin\left(\theta - \frac{\pi}{6} s\right) \\ \theta \end{pmatrix} \tag{32a}$$

amounts to a strong shearing in horizontal direction, bringing the lower boundary of every branch to the right (*i.e.*, to $b = R$), and the upper boundary to the left ($b = -R$), respectively. The second operation is

$$\mathcal{M}_2 : \begin{pmatrix} b \\ \theta \end{pmatrix} \mapsto \begin{pmatrix} b \\ \theta + \pi + 2 \arcsin(\frac{b}{R}) \end{pmatrix}. \tag{32b}$$

The action of the arcsin-function adds an additional phase of 2π to the image of θ, when changing b from $-R$ to $+R$. Thus $\mathcal{M}_2$ represents a shearing in the vertical direction, which leaves the $b = -R$ axis invariant. For instance, the strip $s = 0$ completely traverses the strips $s = 3, \cdots, 9$, has overlap with $s = 1, 2$ and $s = 10, 11$, and only touches $s = 0$ in its two fixed points $(b, \theta) = (\pm R, 0)$. The lacking overlap reflects the "difficulty" to reach the scatterer $s = 0$ in the second collision, when starting from $s = 6$ (cf. Fig. 3). Analogous statements hold for the other branches.

The action of the mapping is schematically described in Fig. 6. For clarity we restrict there to the branches carrying even labels, which are shown as parallelograms, omitting the nonlinear corrections leading to the curved form of the boundaries (27). The piecewise-linear transformations take the form

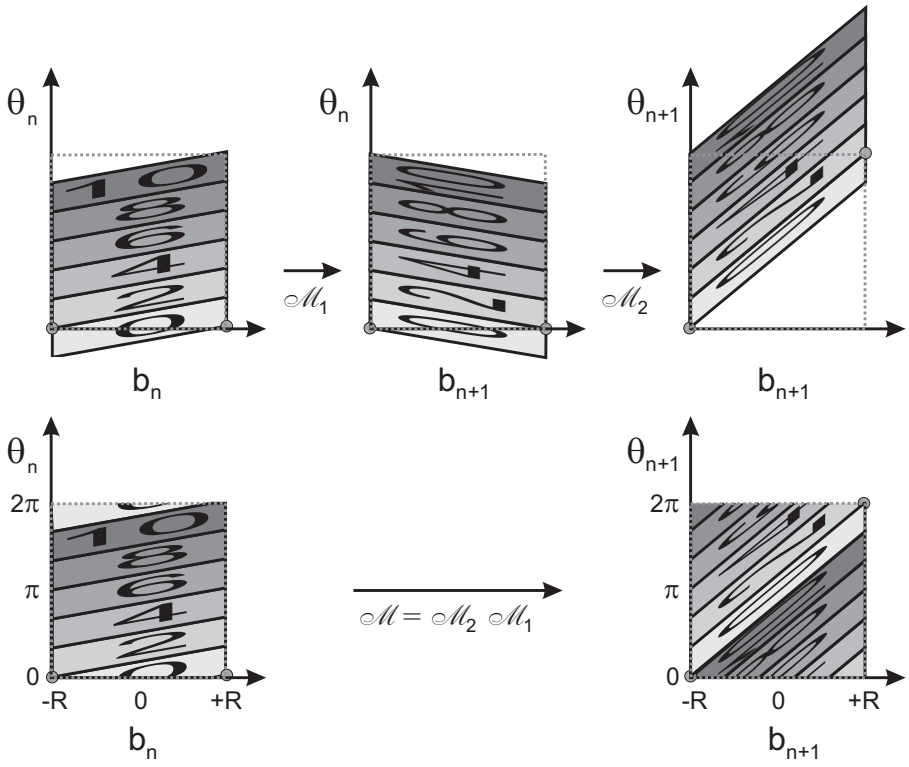

Figure 6: The action of the piecewise linear approximation to the map $\mathcal{M}$. The upper part of the figure shows the action of the linearized $\mathcal{M}_1$ and $\mathcal{M}_2$ given by (33). Their combined action on the fundamental domain is shown in the lower part. The two fixed points of the branch $s = 0$ are indicated by bullets.

$$\mathcal{M}_1 : \begin{pmatrix} b \\ \theta \end{pmatrix} \mapsto \begin{pmatrix} b - l(s) & \left(\theta - \frac{\pi}{6} s\right) \\ & \theta \end{pmatrix}, \tag{33a}$$

and

$$\mathcal{M}_2 : \begin{pmatrix} b \\ \theta \end{pmatrix} \mapsto \begin{pmatrix} b \\ \theta + \pi + 2\frac{b}{R} \end{pmatrix}. \tag{33b}$$

As a result of the combined action of $\mathcal{M}_1$ and $\mathcal{M}_2$, the initial parallelogram is squeezed in the vertical and stretched in the diagonal direction.

Finally we remark that by using the collision map we have lost information on the collision times. They might change in a range but their order of magnitude is set by the lattice distance a and the particle velocity p to $\tau = a/p$. One application of the map therefore corresponds to a time step of length τ.

3.2 Adding an External Field and a Reversible Thermostat. The current of particles in response to an applied external field E has extensively been discussed for the Lorentz gas [3]. In order to avoid an unbounded growth of the energy, the system is typically subjected to a deterministic thermostat fixing the energy (cf. App. A and the review by C. Dettmann in the present volume). The net effect of the field and the thermostat is to change the trajectories in-between collisions from straight line segments to curves of the form (cf. App. A for a derivation)

$$x(t) = x_0 - \frac{p^2}{E} \ln \left[\frac{\cos\left[\theta_0 - E\,(y(t) - y_0)/p^2\right]}{\cos\theta_0} \right], \tag{34}$$

but leaving the modulus of their momentum untouched in spite of the field. Here, (x_0, y_0) is the position of the particle at time $t = 0$, θ_0 is the angle of its initial velocity vector to the y axis, and E is the strength of the applied field, which is taken along the x-direction.

Also in this case the time evolution can be reduced to a mapping relating the initial condition of trajectory segments immediately after subsequent collisions. In this case, however, the angular momentum b of a trajectory segment and the angle θ it has with the y axis are no longer preserved between collisions. As a consequence, the map describing the collisions $\mathcal{M}$ has to be augmented by another one $\mathcal{L}$ describing the evolution of (b, θ) between collisions. The resulting mapping

$$\mathcal{M}^{(E)} \equiv \mathcal{M}\mathcal{L} \tag{35}$$

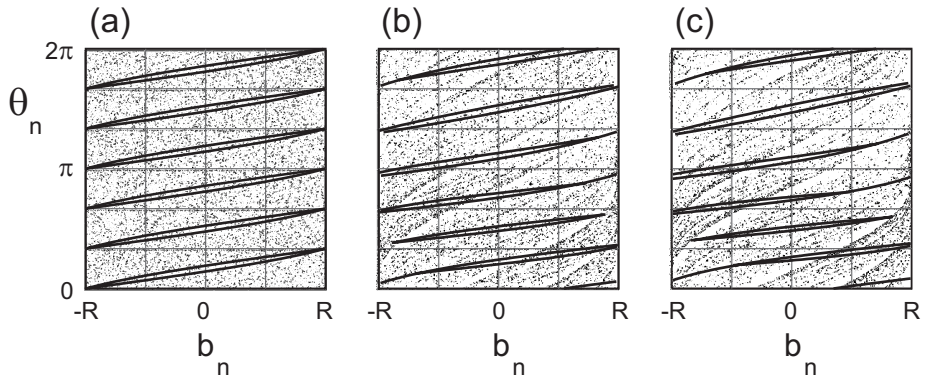

Figure 7: (a) Boundaries of the different branches and their respective images for the mapping $\mathcal{M}^{(E)}$ for (a) $E = 0$, (b) $E = 0.4p^2/a$, and (c) $E = 0.6p^2/a$. The dots in the figures give an impression on the respective invariant densities by showing 20000 iterations of the initial condition $(b, \theta) = (0, 0.1457\pi)$.

remains one-to-one on its domain (cf. Fig. 7) as long as the field is not very strong ($E \lesssim 4.5p^2/a$, cf. [58]). However, the boundaries of the different branches can no longer be calculated analytically. The numerical solution for the shape of the branches and their images for different field strengths is shown in Fig. 7. We mention that collisions with the six unmarked disks of Fig. 3 also occur but in so tiny regions that they cannot be resolved in Fig. 7b and c. Since the modulus of the momentum has not changed, the time unit remains $\tau = a/p$.

The dynamics of the Lorentz gas in the presence of an external field is still invariant under reflections at the horizontal axis parallel to the field, which amounts to the symmetry $(b, \theta) \to (R - b, 2\pi - \theta)$ observed by the map $\mathcal{M}^{(E)}$. Moreover, since the collision operator $\mathcal{M}$, as well as the evolution, $\mathcal{L}$ are time reversal invariant (cf. App. A), the involution $\mathcal{T}$ generates the time reversed motion also for $\mathcal{M}^{(E)}$, at least for sufficiently small E.

On the other hand, the field breaks the discrete rotational invariance of the mapping $\mathcal{M}^{(E)}$. As a consequence, the branches of the map become different in area. From Fig. 7, one checks that the branches to be mapped in the direction of the field ($s = 7 \cdots 11$) are now larger than those mapped opposite to the field ($s = 1 \cdots 5$). However, since the time-reversal operator is area preserving, the area of the image of the branch s exactly matches the area of branch $[s{+}6]\mathrm{mod}12$. Consequently, $\mathcal{M}^{(E)}$ expands (contracts) area when moving in (opposite to) the direction of the field, *i.e.*, the mapping $\mathcal{M}^{(E)}$ does no longer preserve the phase-space volume. This is indeed expected, since the evolution operator $\mathcal{L}$ expands (contracts) area, when moving in (opposite to) the direction of the field (as shown in App. A). As a consequence of the phase-space contraction and expansion the natural invariant density is no longer uniform. This is exemplified by the complicated asymptotic structure of the density sampled by a single typical trajectory in Fig. 7. A typical trajectory is more often mapped into the direction of the field than opposite to it (cf. Fig. 7, where the strips 7–9 carry more particles than 1–5). This leads to a particle current induced by the applied field, and a closely related average phase-space contraction. The properties of this response have been studied in Refs. [7, 58, 59].

3.3 The Spatially-Extended Lorentz Gas. In addition to systems with periodic boundary conditions, our interest is the modeling of spatially extended systems, where transport can also be induced by imposing flux boundary conditions. These are called open systems. In this situation not even the stationary densities are uniform in the direction of transport, *i.e.*, along the x axis. There is only translation invariance parallel to the y axis, and one explicitly has to keep track of the motion of the particles in the x direction. An appropriate way of doing this in the Lorentz gas is to view the array of scatterers as a sequence of columns parallel to the y axis (cf. Fig. 3). Within these columns the scatterers are not distinguished. We consider a system of fixed length $L \equiv Na$ in the x direction. Also in this situation the time evolution of a trajectory can be described by a mapping, but now its domain consists of $N + 4$ columns. These

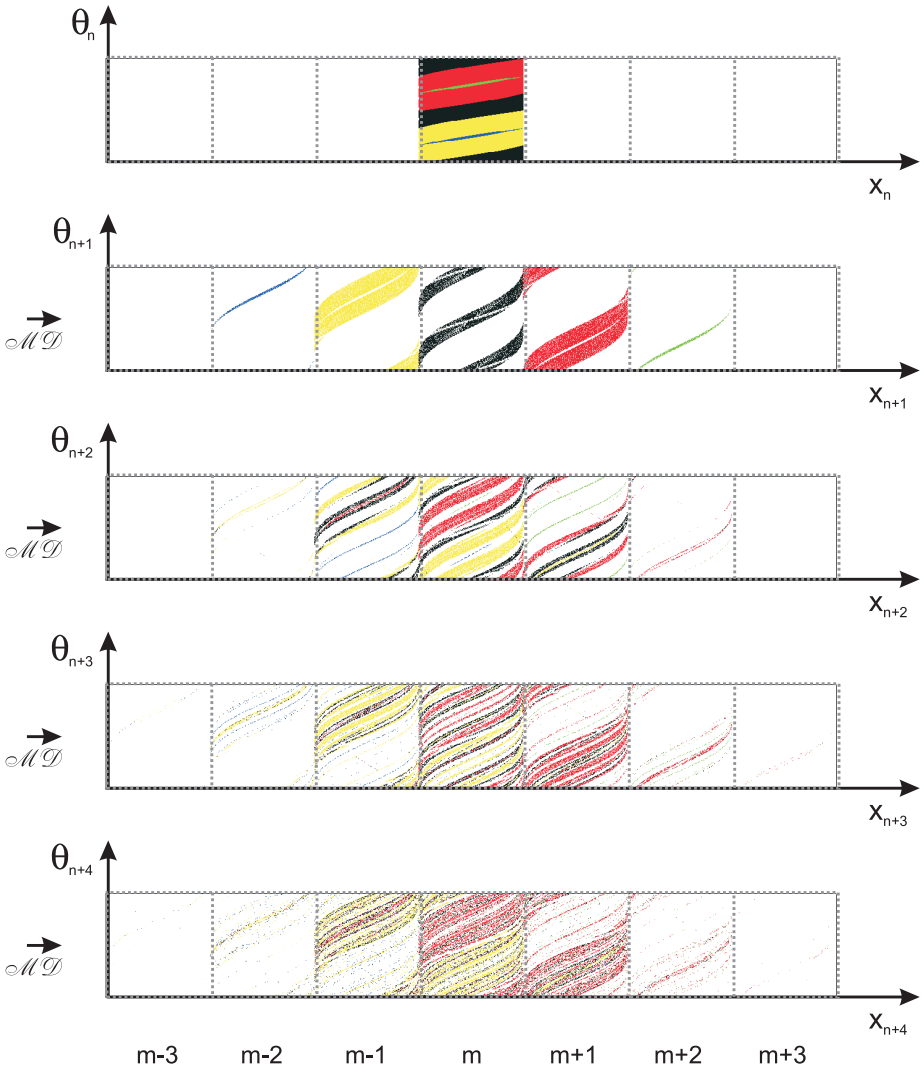

Figure 8: Action of the mapping $\mathcal{M}^{(O)}$ for $E = 0$ where the spatial information of the position of the scatterer is kept for the x-direction only. All initial conditions lie in cell m, and under the mapping they are redistributed among neighboring cells. The initial conditions which are mapped to cell $m-2$ $(m+2)$ in the first time step are colored blue (green), those mapped to cell $m-1$ $(m+1)$ are colored yellow (red) and the ones staying in cell m are black.

columns will be called *cells* in the following. They are labelled by the index $m = -1, 0, 1, \cdots, N, N+1, N+2$, such that their sequence reflects the progression of the columns of scatterers. The columns $m = -1, 0$ and $m = N+1, N+2$ are needed to implement the boundary conditions. In addition to the pairs (b_n, θ_n) one now has to specify the column m_n, where the n^{th} collision takes place. A convenient way to describe this dynamics is to extend the mapping $\mathcal{M}$ to a chain of mutually connected cells (Fig. 8), where the map with index m_n is applied when the n^{th} collision takes place in cell m_n. The horizontal coordinate of the mapping is thus $x_n \equiv a\ m_n + b_n$, while the vertical coordinate remains θ_n. In the cells $m = -1,\ 0,\ N+1$, and $N+2$ special rules are employed to realize the boundary conditions. The new mapping $\mathcal{M}^{(O)}$ describing the time evolution between the nth and $(n+1)$st collision

$$\mathcal{M}^{(O)} \equiv \mathcal{M}^{(E)}\mathcal{D} \tag{36}$$

comprises a displacement $\mathcal{D}$ between the cells in addition to the mapping $\mathcal{M}^{(E)}$ relating the coordinates (b, θ) of successive collisions. The displacement $\mathcal{D}$ acts as follows in the different branches of $\mathcal{M}^{(O)}$ (cf. the upper two rows of Fig. 8 for an illustration of the action of $\mathcal{M}^{(O)}$):

$s = 3$ This branch is mapped from cell m to $m-2$. The space taken by the image of the $s = 3$ branch in Fig. 5 is taken now by points with their preimages in cell $m+2$.

$s \in \{1, 2, 4, 5\}$ The branches are mapped from cell m to $m-1$. The corresponding space taken by their respective images in Fig. 5 is taken by points with their preimages in cell $m+1$.

$s \in \{0, 6\}$ The trajectories proceeding to scatterers labeled by $s = 0$ or $s = 6$ are not displaced in the direction of transport. The corresponding branches are mapped into the initial cell m itself.

$s \in \{7, 8, 10, 11\}$ The branches of the map are mapped from cell m to $m+1$. The corresponding space taken by their respective images in Fig. 5 is taken by points with preimages in cell $m-1$.

$s = 9$ The branch of the map carrying the label $s = 10$ is mapped from cell m to $m+2$. The space taken by the image of the $s = 10$ branch in Fig. 5 is taken now by points with their preimages in cell $m-2$.

In Fig. 8 the resulting dynamics is followed over four time steps for initial conditions in cell m. Points starting in different branches of $\mathcal{M}^{(O)}$ are indicated by different colors. In the first step the images of the various branches of the map can still clearly be distinguished, but after only a few time steps they are stretched and mixed up so strongly that this is no longer possible in a graphical illustration of this type. The motion of the shown initial condition appears to

be diffusion like from this representation. This property is a direct consequence of the displacement operation $\mathcal{D}$ acting on top of the chaotic dynamics $\mathcal{M}^{(E)}$ (as initially shown for spatially extended one-dimensional maps [60]).

3.4 Symbolic Dynamics and Pruning. The observation of diffusive-like motion of particles in the extended Lorentz gas can be encoded by a symbolic dynamics. To this end the trajectories are represented by symbol sequences specifying the order a trajectory visits the scatterers. By this approach one rigorously links the time evolution $\mathcal{M}^{(O)}$ to the one of a random walk (with an exponentially decaying memory). The particle trajectories are encoded by specifying the scatterer hit at collision $n+1$ [at approximate time $(n+1)\tau$] by the symbol s_n. The code can take on any of the symbols defined in Fig. 3. Thus, one arrives at the symbol sequence $\cdots s_{-3}\, s_{-2}\, s_{-1} \bullet s_0\, s_1\, s_2 \cdots$. In this way, the full sequence describes how a trajectory proceeds forward and backward in time from a given disk. Application of the map $\mathcal{M}^{(O)}$ corresponds to shifting the $\bullet$ one position to the right. Regions in the fundamental domain obtained by intersecting the k^{th} preimages of the branches with their l^{th} images contain by construction all those (allowed) sequences which share a given middle part of the symbol sequence with k (l) symbols before (after) the $\bullet$. For hyperbolic systems these regions contract to points in the limit $k, l \to \infty$, *i.e.*, every trajectory in the system is uniquely characterized by a symbol sequence.

We stress, that not all sequences represent allowed trajectories. For instance, it was argued above that for $E = 0$ a trajectory cannot proceed to $s = 0$ in two successive collisions. As a consequence, no pairs of two neighboring identical symbols can appear in an admissible sequence. This necessity to rule out unphysical symbol sequences is called *pruning* in the physical literature [44]. A full characterization of the dynamics requires to specify the set of allowed symbols as well as the *grammatical rules* specifying the admissible sequences. There are changes in these rules whenever the system undergoes a bifurcations in the course of changing parameters such as the external field E. The prevalence of bifurcations leads to a complex (fractal) dependence of transport properties of the Lorentz gas on the parameters, which is a typical feature of transport in low-dimensional dynamical systems. These complicated dependences are in our eyes non-thermodynamic features, which we will not further discuss in the following. They have been studied in detail in Refs. [61, 62].

The importance of the symbolic dynamics lies in the relation it establishes between the invertible microscopic dynamics of the particle system and a stochastic, random-walk like process defined by a Markov graph on the space of admissible symbol sequences (cf. [44, 63] for details). By this approach the diffusive spread of the initial conditions observed in Fig. 8 can thus directly be related to the one of random walkers on the line. The continuum limit of this discrete stochastic process, we relate to the transport equations. This allows us to go from the deterministic microscopic dynamics to the related thermodynamic description of transport in a well-defined sequence of steps. We emphasize that

a full thermodynamic description requires not only the transport equations but a consistent entropy balance, too. A discussion of this relation will be the aim of the next Section. First, however, we introduce a simplifying condition which makes analytic computation possible.

3.5 Piecewise-Linear Approximation of the Lorentz Dynamics. Details of the long-time dynamics and of the transport properties of the Lorentz gas are difficult to deal with analytically due to the complexity of the mapping $\mathcal{M}^{(O)}$. In order to understand generic features of models based on dynamical systems it is therefore helpful to consider the spatially extension of the linearized version (33) of the map introduced in Fig. 6. In Fig. 9 the resulting dynamics is followed over two time steps for initial conditions in cell m. The branches are indicated by the respective values of the (even) symbols s. The evolution of the shown initial condition appears to be diffusion like from this representation, too. Again, this property is a direct consequence of the displacement operation $\mathcal{D}$ acting on top of the chaotic dynamics, but in this case the dynamics is described by a piecewise-linear mapping. Note that there is still pruning, however.

3.6 The Next-To-Nearest-Neighbor (nnn) Multibaker Map. The occurrence of pruning and of correlations between successive jumps are technical difficulties, which need not be considered when trying to clarify conceptual problems. A slight geometrical change of the map of Fig. 9 leads to the disappearance of pruning without modifying the overall features. This change corresponds to choosing the boundaries of the map's branches to coincide with the local stable and unstable manifolds. The new coordinate orthogonal to the x axis (the analog of θ) is denoted by p and can take on values in the interval $[0, b]$ where b is an arbitrary positive number. The variable p is momentum-like. It is perpendicular to the transport direction and generates fractal structures. Note, however, that p is not conjugated to x in the sense of classical mechanics. The contracting (expanding) direction is now parallel to the p (x) axis. The map $\mathcal{B}$ obtained in this way is called a next-to-nearest-neighbor (nnn) multibaker map since there are next-to-nearest-neighbor transitions of particles. It is defined graphically in Fig. 10 and 11. Its time unit τ is the same as for the previous maps.

Similarly to the extended Lorentz gas the phase space of the multibaker map $\mathcal{B}$ consists of a chain of identical cells of linear size a and area $\Gamma = a \times b$ (cf. Fig. 10). The dynamics is the same on each cell, except for possibly the outermost ones (-1, 0, $N+1$, $N+2$), where boundary conditions are imposed.

The map $\mathcal{B}$ is piecewise linear and defined on a set of branches partitioning each cell. Every branch is compressed in the vertical and stretched in the horizontal direction. The images are translated to neighboring cells or are rearranged in the original cell (cf. Fig. 10). More precisely, every cell is divided into 5 vertical columns (see Fig. 11). The rightmost (leftmost) column of width $r_2 a$ ($l_2 a$) of each cell is mapped onto a strip of width a and height $\tilde{r}_2 b$ ($\tilde{l}_2 b$) in the second cell to the right (left). The inner right (left) column of width $r_1 a$ ($l_1 a$) of each cell is mapped onto a strip of width a and height $\tilde{r}_1 b$ ($\tilde{l}_1 b$) in the neighboring cell to

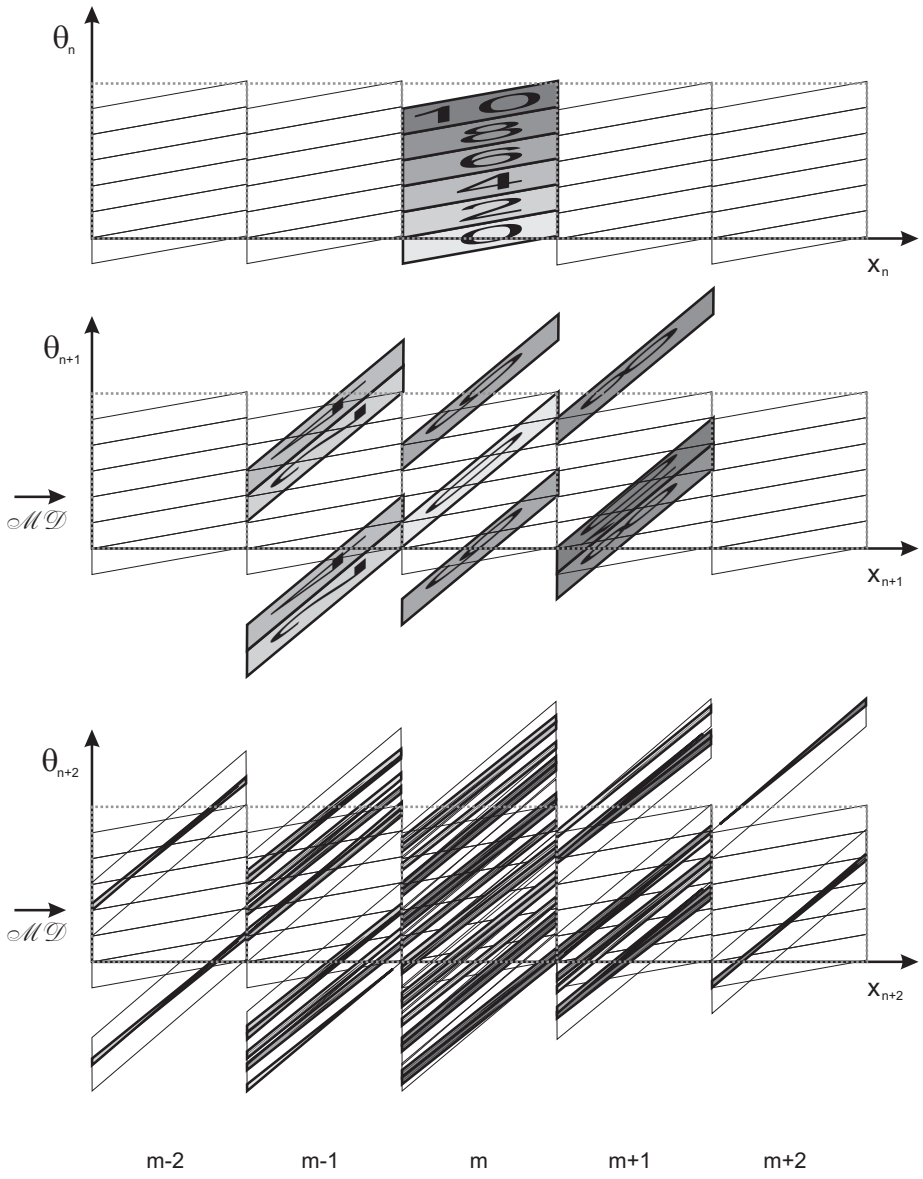

Figure 9: Map $\mathcal{M}^{(O)} = \mathcal{MD}$ based on the piecewise-linear approximation of the field free case $\mathcal{M}$ introduced in Fig. 6, which neglects trajectories to next-to-nearest neighbors. All initial conditions lie in cell m, and under the mapping they are redistributed among neighboring cells.

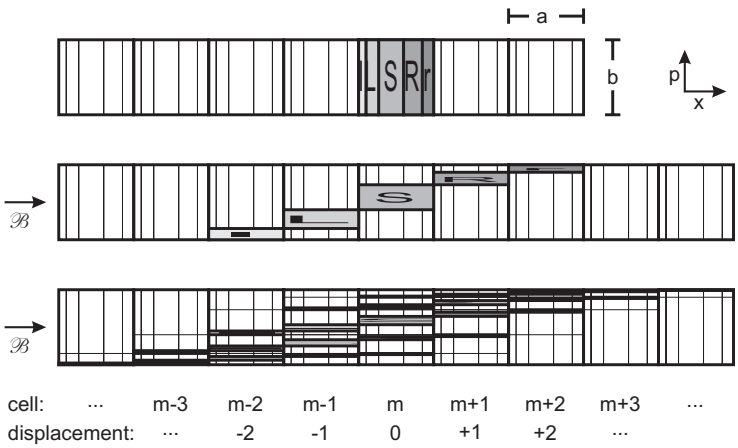

Figure 10: Sketch of the next-to-nearest-neighbor multibaker map. The mapping is the same in each of the inner cells $m = 1 \cdots N$, and acts after time units τ. Its branches are marked by different shades of gray and indicated by the letters l, L, S, R, r, in order to demonstrate the action over two time steps on initial conditions in cell m. The mapping connects the cell m with its neighbors $m \pm 1$ and next-to-nearest neighbors $m \pm 2$ as described in the text (also cf. Fig. 11). Displacements are measured in units of a.

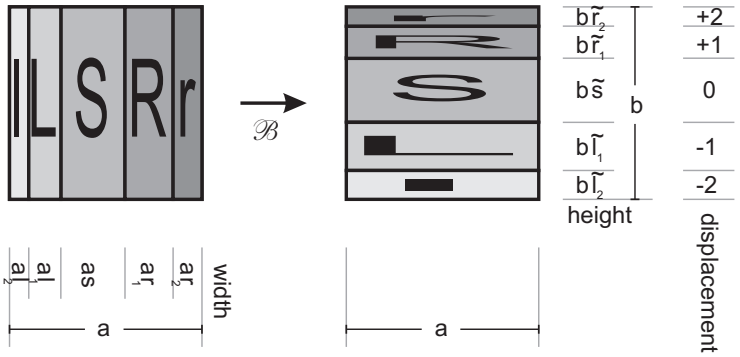

Figure 11: Sketch of the next-to-nearest-neighbor multibaker dynamics. Five vertical columns of height b are squeezed and stretched to obtain horizontal strips of width a, which are displaced to neighboring cells. The width and height of the respective strips is given at the margin of the plot. The respective displacement, measured in units of a, is given to the right. The letters (l,L,S,R,r) are meant to illustrate the action of the map on the different columns; they do not correspond to the widths of the columns.

the right (left). These columns are responsible for transport in one time step τ. The middle column of width sa stays inside the cell, thus modeling the motion that does *not* contribute to transport during a single iteration. This column is mapped onto a strip of width a and height $\tilde{s}b$. The internal dynamics is chosen to be area preserving, i.e., $s = \tilde{s}$. In analogy to the Lorentz gas we require *global* phase-space conservation, which implies the sum rules

$$l_1 + r_1 + l_2 + r_2 = 1 - s = 1 - \tilde{s} = \tilde{l}_1 + \tilde{r}_1 + \tilde{l}_2 + \tilde{r}_2. \tag{37}$$

Altogether, the multibaker dynamics is governed by the mapping (for convenience x is measured here with respect to the left corner of cell m)

$$\mathcal{B} : (x,p) \mapsto \begin{cases} \left(\frac{x-am}{l_2} + (m-2)\,a, \quad b\tilde{l}_2 p \right) \\ \text{for } 0 < \frac{x}{a} - m < l_2 \\ \left(\frac{x-a(m+l_2)}{l_1} + (m-1)\,a, \quad b\tilde{l}_2 + \tilde{l}_1 p \right) \\ \text{for } l_2 < \frac{x}{a} - m < l_2 + l_1 \\ \left(\frac{x-a(m+l_2+l_1)}{s} + m, \quad b(\tilde{l}_2 + \tilde{l}_1) + \tilde{s}p \right) \\ \text{for } l_1 + l_2 < \frac{x}{a} - m < l_2 + l_1 + s \\ \left(\frac{x-a(m+l_2+l_1+s)}{r_1} + (m+1)\,a, \quad b(\tilde{l}_2 + \tilde{l}_1 + \tilde{s}) + \tilde{r}_1 p \right) \\ \text{for } l_2 + l_1 + s < \frac{x}{a} - m < 1 - r_2 \\ \left(\frac{x-a(m+1-r_2)}{r_2} + (m+2)\,a, \quad b(1-\tilde{r}_2) + \tilde{r}_2 p \right) \\ \text{for } 1 - r_2 < \frac{x}{a} - m < 1. \end{cases} \tag{38}$$

Using the Frobenius-Perron operator [4, 44] this completely specifies the time evolution of the phase-space density $\varrho(x,p)$.

It is worth introducing a short-hand notation p_i for the transition probabilities from a given cell to its ith neighbor (cf. Fig. 10). Since the dynamics is assumed to be translation invariant along the chain, these rates do not depend on m. The transition probabilities p_i taken with respect to a uniform cell density from cell m to cell $m+i$ are proportional to the width of the columns. In view of the definition of the map, we have

$$p_i = \begin{cases} l_2 & \text{for} \quad i = -2 \\ l_1 & \text{for} \quad i = -1 \\ s & \text{for} \quad i = 0 \\ r_1 & \text{for} \quad i = 1 \\ r_2 & \text{for} \quad i = 2. \end{cases} \tag{39}$$

In a similar fashion, the quantity $\tilde{p}_i$ is a shorthand notation for the parameters characterizing the height of the horizontal strips in (38).

Similarly to the approach taken for the Lorentz system, we call the (x, p) dynamics of the multibaker map time reversible if there is an involution $\mathcal{T}_\mathcal{B}$ such that

$$\mathcal{B}^{-1} = \mathcal{T}_\mathcal{B} \mathcal{B} \mathcal{T}_\mathcal{B}, \tag{40}$$

which fulfill the additional constraints that (i) it acts only locally, i.e., it maps points only within cells, (ii) it is area preserving, and (iii) it is independent of the bias $r_1 - l_1$ or $r_2 - l_2$ modeling the presence of an external field. These conditions can only be fulfilled provided that the area Γp_i of the strip mapped i cells to the right exactly matches the area $\Gamma \tilde{p}_{-i}$ of the image of the strip mapped i cells to the left, i.e., if

$$p_i = \tilde{p}_{-i} \quad \text{for every } i. \tag{41}$$

The time reversibility of the multibaker map can in this case be expressed like in Eq. (29) by applying the time-reversal operation

$$\mathcal{T}_\mathcal{B} : (x, p) \mapsto \left(a\,(1 - \frac{p}{b}), b\,(1 - \frac{x}{a}) \right) \tag{42}$$

in every cell (x is taken here mod a to avoid writing out the trivial dependence on the cell index). Equation (41) constitutes the only choice of parameters of the considered multibaker map, where a time-reversal operator complying with the above requirements can be found. It covers the area-preserving dynamics without bias, but even the biased area-preserving dynamics is excluded from the class of time reversible dynamics.

§4. Transport and Entropy Production in the (nnn) Multibaker Map

In multibaker chains it is natural to carry out coarse graining within the cells. Let

$$\varrho_m \equiv \frac{1}{\Gamma} \int_{\text{cell } m} \mathrm{d}x\, \mathrm{d}p\, \varrho(x, p) \tag{43}$$

be the coarse-grained density in cell m. It will be called *cell density* in the following. The conservation of particle number leads to a master equation relating the density after one time step ϱ'_m to the initial densities ϱ_m [64]:

$$\varrho'_m = \sum_i p_i \varrho_{m-i}. \tag{44}$$

Here and in the following primed quantities denote quantities taken after one time step τ.

4.1 Time Evolution of the Entropies. The cell density ϱ_m is a coarse-grained density in the spirit of Sect. 2 taken with respect to boxes correspond to the cells of the multibaker map. The resulting coarse-grained entropy is

$$S_m = -\Gamma\ \varrho_m \ln\left(\frac{\varrho_m}{\varrho^\star}\right), \tag{45}$$

where $\varrho^\star$ is a constant reference density. By definition, the coarse-grained entropy after time τ is $S'_m = -\Gamma\ \varrho'_m \ln(\varrho'_m/\varrho^\star)$.

We assume that in the initial configuration the phase-space density is constant in each cell: $\varrho_0(x,p) = \varrho_m$. Consequently, the coarse-grained and the Gibbs entropy $S_m^{(\mathrm{G})}$ agree initially. In order to compute the Gibbs entropy $S_m^{(\mathrm{G})'}$ after time τ, we observe that the number of particles evolving with a given branch of the map is preserved. Thus, the density changes due to the changes of the phase-space volume only, which are described by the *contraction factors* $\tilde{p}_i/p_i$. This leads to the new densities

$$\varrho'_{m,i} = \frac{p_i}{\tilde{p}_i}\varrho_{m-i} \tag{46}$$

on the strips of volume $\tilde{p}_i\Gamma$ of cell m. Note that the density is preserved for volume elements mapped within cell m, i.e., $\varrho'_{m,0} = \varrho_m$. The Gibbs entropy is thus

$$\begin{aligned} S_m^{(\mathrm{G})'} &\equiv -\sum_i \Gamma\tilde{p}_i\varrho'_{m,i}\ \ln\left(\frac{\varrho'_{m,i}}{\varrho^\star}\right) \\ &= -\sum_i \Gamma p_i\varrho_{m-i}\ \ln\left(\frac{\varrho_{m-i}}{\varrho^\star}\frac{p_i}{\tilde{p}_i}\right) \\ &= \Gamma\left[-\varrho'_m \ln\frac{\varrho_m}{\varrho^\star} - \sum_i p_i\varrho_{m-i}\ln\left(\frac{\varrho_{m-i}}{\varrho_m}\frac{p_i}{\tilde{p}_i}\right)\right] \end{aligned} \tag{47}$$

where (44) has been used to arrive at the last equation. The irreversible entropy change, the discrete time analog of (16), becomes

$$\begin{aligned} \Delta_i S_m &\equiv (S'_m - S_m^{(\mathrm{G})'}) - (S_m - S_m^{(\mathrm{G})}) = S'_m - S_m^{(\mathrm{G})'} \\ &= \Gamma\left[\sum_i p_i\varrho_{m-i}\ln\left(\frac{\varrho_{m-i}}{\varrho_m}\frac{p_i}{\tilde{p}_i}\right) - \varrho'_m\ \ln\left(\frac{\varrho'_m}{\varrho_m}\right)\right]. \end{aligned} \tag{48}$$

We remark that these expressions are valid even for more general multibaker maps, where non-vanishing transition probabilities p_i and corresponding phase-space contraction factors $\tilde{p}_i/p_i$ appear for arbitrarily long jumps. For concreteness, we restrict ourselves, however, to treating the next-to-nearest-neighbor map only, for which p_i and $\tilde{p}_i$ vanish for $|i| > 2$.

4.2 The Macroscopic Limit for Transport and the Advection-Diffusion Equation. After having derived exact results for the coarse-grained density and the irreversible entropy production, we evaluate them in the macroscopic limit. In thermodynamics one is interested in the large-system limit $a \ll L$. This corresponds to observing the transport process on a macroscopic length scale, comparable with L. In a mathematical idealization, where one disregards the discreteness of cells, this limit corresponds to $a \to 0$. In this limit the spatial variation of the densities described by the discrete index m reduces to a functional dependence on the continuous variable $x = ma$.

Since the coarse graining corresponds in our case to integrating out the momentum variable, the spatial variation of the particle density $\rho_m \equiv b\varrho_m$ follows the one of the coarse-grained phase-space density ϱ_m. In the large-system limit, the cell densities for the neighbors of cell m [*i.e.*, at positions $x \pm dx = (m\pm1)a$] can thus be expressed through spatial derivatives of the particle-density distribution $\rho(x)$ at $x = ma$. Up to second order in a one obtains

$$b\varrho_{m\pm1} = \rho(x) \pm a\partial_x\rho(x) + \frac{a^2}{2}\,\partial_x^2\rho(x). \tag{49}$$

This yields for the temporal variation of the cell density [cf. (44)]

$$\begin{aligned} \frac{\rho'(x) - \rho(x)}{\tau} &\equiv \frac{b(\varrho'_m - \varrho_m)}{\tau} \\ = -\frac{a}{\tau}\left[r_1 - l_1 + 2(r_2 - l_2)\right]\,\partial_x\rho &+ \frac{a^2}{2\tau}\left[r_1 + l_1 + 4(r_2 + l_2)\right]\,\partial_x^2\rho. \end{aligned} \tag{50}$$

In the limit $\tau \to 0$, Eq. (50) goes over into an advection-diffusion equation

$$\partial_t\rho(x) = -\partial_x[v\rho(x) - D\partial_x\rho(x)] \tag{51}$$

with a drift

$$v \equiv v_1 + v_2 = \frac{a}{\tau}[r_1 - l_1] + \frac{a}{\tau}2[r_2 - l_2], \tag{52a}$$

and a diffusion coefficient

$$D \equiv D_1 + D_2 = \frac{a^2}{2\tau}[r_1 + l_1] + \frac{a^2}{\tau}2[r_2 + l_2]. \tag{52b}$$

Here v_i (D_i), $i = 1, 2$, represent the 'partial' drift (diffusion) coefficients, characterizing contributions from nearest and from next-to-nearest-neighbor

transitions, respectively. Eq.(51) is the desired transport equation describing (particle) transport in the context of multibaker maps. The particle current is found to be

$$j = v\varrho(x) - D\partial_x \varrho(x). \tag{53}$$

In order to have a well-defined transport equation with finite parameters v and D, the differences of the respective transition rates should scale as a/τ, and their sums as a^2/τ. The macroscopic limit required to derive (51) corresponds to $a, \tau \to 0$ with v and D fixed.

4.3 The Macroscopic Limit for the Entropy Balance. The condition for the existence of an advection-diffusion equation requires the finiteness of v and D, and thus of the combinations (52) only. These are two relations on the four transition rates and leave the four independent heights fully unconstrained. The existence of a thermodynamically consistent entropy balance heavily depends, however, on a proper scaling of the heights.

First, based on a physical constraint, we give a one-parameter scaling form of the transition rates. It is well-known in the theory of stochastic processes [45, 64] that v/D is proportional to the external field. Since the field is assumed to be constant along the chain, we impose as an additional condition on the microscopic dynamics that the relation v_i/D_i is independent of i. This leads to the condition

$$\frac{r_1 - l_1}{r_1 + l_1} = \frac{1}{2}\frac{r_2 - l_2}{r_2 + l_2}. \tag{54}$$

Therefore, one parameter, denoted in the following by α, can still freely be chosen when expressing r_1, r_2, l_1, l_2 by a, τ, v and D. A convenient form of the representation is

$$r_1 = \frac{\tau D}{a^2}\alpha\left(1 + \frac{a\ v}{2D}\right), \quad l_1 = \frac{\tau D}{a^2}\alpha\left(1 - \frac{a\ v}{2D}\right), \tag{55a}$$

and

$$r_2 = \frac{\tau D}{a^2}\frac{1-\alpha}{4}\left(1 + \frac{a\ v}{D}\right), \quad l_2 = \frac{\tau D}{a^2}\frac{1-\alpha}{4}\left(1 - \frac{a\ v}{D}\right). \tag{55b}$$

This form ensures the existence of a well-defined macroscopic transport equation, irrespective of the value of α. However, it remains to be seen whether also meaningful expressions for the irreversible entropy production are found.

While the transport equation is independent of the phase-space contraction factors $\tilde{p}_i/p_i$, these ratios do show up in the irreversible entropy production (48). After all, the irreversible entropy production is sensitive to dissipation in the deterministic chaotic dynamics describing the corresponding microscopic evolution. To parameterize these dependences, it is convenient to introduce a representation for the $\tilde{p}_i$ analogous to (55):

$$\tilde{r}_1 = \frac{\tau D}{a^2}\beta\alpha\left(1+\varepsilon_1\frac{a\ v}{2D}\right), \quad \tilde{l}_1 = \frac{\tau D}{a^2}\beta\alpha\left(1-\varepsilon_1\frac{a\ v}{2D}\right) \tag{56a}$$

and

$$\tilde{r}_2 = \frac{\tau D}{a^2}\gamma\frac{1-\alpha}{4}\left(1+\varepsilon_2\frac{a\ v}{D}\right), \quad \tilde{l}_2 = \frac{\tau D}{a^2}\gamma\frac{1-\alpha}{4}\left(1-\varepsilon_2\frac{a\ v}{D}\right). \tag{56b}$$

Here, $\beta > 0$, $\gamma > 0$, ε_1 and ε_2 are parameters characterizing the dissipation in the system. The coefficient γ can be expressed by α and β, since due to (37) the sum of the p_i equals that of the $\tilde{p}_i$ leading to $4\alpha\beta + (1-\alpha)\gamma = 1 + 3\alpha$.

When applying the condition of time reversibility (41) to the parameters, we find from (55) and (56) two conditions: (i) $\beta = \gamma = 1$, and (ii) $\varepsilon_i = -1$. This choice corresponds to a dissipative, time-reversible biased dynamics, similar to the one of the Lorentz gas subjected to an external field with a reversible thermostat.

Since the parameters α, β, γ, ε_1 and ε_2 are also relevant for the macroscopic behavior we *define* the macroscopic limit as:

$$a \to 0, \quad \tau \to 0, \quad \text{with} \quad v,\ D,\ \varepsilon_i, \alpha, \beta \quad \text{fixed}. \tag{57}$$

4.4 Entropy Production in the Macroscopic Limit. Substituting relation (50) into (48) yields for the irreversible entropy production in the large system limit $a \to 0$

$$\frac{\Delta_i S_m}{a\tau} = \bar{\sigma}\rho - a(\sigma_+ - \sigma_-)\,\partial_x\rho + \left(D - \frac{\tau}{2}v^2\right)\frac{(\partial_x\rho)^2}{\rho} + O\left(\bar{\sigma}a^2\partial_x^2\rho\right). \tag{58}$$

Here,

$$\bar{\sigma} \equiv -\frac{1}{\tau}\left[l_2 \ln\frac{\tilde{l}_2}{l_2} + l_1 \ln\frac{\tilde{l}_1}{l_1} + r_1 \ln\frac{\tilde{r}_1}{r_1} + r_2 \ln\frac{\tilde{r}_2}{r_2}\right] \tag{59}$$

is the average phase-space contraction rate for a homogeneous phase-space density distribution. Furthermore,

$$\sigma_+ \equiv -\frac{1}{\tau}\left[r_1 \ln\frac{\tilde{r}_1}{r_1} + 2r_2 \ln\frac{\tilde{r}_2}{r_2}\right] \tag{60}$$

is an average phase-space contraction rate for the motion in the positive direction. σ_- is defined in an analogous way by replacing r via l in the formula. The first two terms of (58) are consequences of the phase-space contraction, while the third one arises from the mixing between neighboring cells and from the time evolution. The fact that these equations are expressed solely by spatial derivatives of the particle-density distribution does not yet ensure the existence of a well-defined macroscopic limit for the rate of irreversible entropy production

$$\frac{\Delta_i S_m}{a\tau} \to \sigma^{(\mathrm{irr})} \tag{61}$$

and other quantities. The result obtained in the limit $\tau \to 0$ strongly depends on how the transition probabilities p_i behave. Using (55), (56), in the macroscopic limit (57) one immediately finds

$$\bar{\sigma} = -\frac{D}{a^2}\left[\alpha \ln\beta + \frac{1-\alpha}{4}\ln\gamma\right] + \frac{v^2}{4D}\left[\alpha(1-\varepsilon_1)^2 + (1-\alpha)(1-\varepsilon_2)^2\right], \tag{62a}$$

and

$$a(\sigma_+ - \sigma_-) = v\left[\alpha(1-\varepsilon_1) + (1-\alpha)(1-\varepsilon_2)\right]. \tag{62b}$$

Note that the relation for $\bar{\sigma}$ diverges in the limit $a \to 0$ unless one requires $\beta = \gamma = 1$. This shows that the finiteness of the average phase-space contraction cannot be ensured in the model without the first necessary condition (i) on time reversibility. Observing this requirement when inserting the relations (62), as well as (55) and (56), into Eq. (48) one obtains

$$\begin{aligned}\sigma^{(\mathrm{irr})}(\varepsilon_i) &= \frac{\rho}{D}\left\{\frac{v^2}{4}\left[\alpha(1-\varepsilon_1)^2 + (1-\alpha)(1-\varepsilon_2)^2\right]\right. \\ &\qquad \left. -vD\ \left[\alpha(1-\varepsilon_1) + (1-\alpha)(1-\varepsilon_2)\right]\frac{\partial_x\rho}{\rho} + D^2\left(\frac{\partial_x\rho}{\rho}\right)^2\right\} \\ &= \frac{\rho}{D}\left\{\alpha\ \left[\left(\frac{1-\varepsilon_1}{2}\right)\ v - D\frac{\partial_x\rho}{\rho}\right]^2\right. \\ &\qquad \left. +(1-\alpha)\ \left[\left(\frac{1-\varepsilon_2}{2}\right)\ v - D\frac{\partial_x\rho}{\rho}\right]^2\right\}. \end{aligned} \tag{63}$$

Whether it coincides with the thermodynamic results still depends, however, on the parameters ε_1 and ε_2. According to thermodynamics, the rate of irreversible entropy production in a system with drift and diffusion is $j^2/(\rho D)$ where j is the particle-current density. Hence,

$$\sigma^{(\mathrm{irr})} = \frac{\rho}{D}\left[v - D\frac{\partial_x\rho}{\rho}\right]^2. \tag{64}$$

A coincidence can only be ensured if the dissipation parameters are properly chosen. One immediately sees that $\varepsilon_1 = \varepsilon_2 = -1$ is the *only* choice of parameters where agreement with thermodynamics is possible. The agreement is then found independently of the choice of the parameter α. Altogether we find that only a time reversible dissipative dynamics is able to lead to the thermodynamic results.

§5. Results Obtained with (nn) Multibaker Maps

Since the probability to jump to a next-to-nearest-neighbor cell in the Lorentz gas is rather low, the dynamics can faithfully be approximated by a nearest-neighbor (nn) multibaker map. Research has mainly concentrated on this type of multibaker maps, i.e., on the special case $l_2 = r_2 = \tilde{r}_2 = \tilde{l}_2 = 0$ of Eq. (38). Here we summarize results obtained for different problems related to irreversibility and transport. Doing this, we consider cases with a reversible dissipation mechanism only, i.e., with $\tilde{l} = r$ and $\tilde{r} = l$ (the subscript 1 of l, r, $\tilde{l}$ and $\tilde{r}$ is suppressed in the following). It is in general true that besides this case one cannot find agreement with Irreversible Thermodynamics. Earlier results on unbiased area-preserving multibakers (i.e., for the special case $r = l = \tilde{r} = \tilde{l}$) have been reviewed in [4].

5.1 Invariant Densities and Takagi Functions. The average densities in the cells of a multibaker chain evolve according to a master equation (44). The stationary density profile with fixed densities ϱ_0 and ϱ_{N+1} at the left and right boundary of the chain, respectively, fulfills

$$\varrho_m = \varrho_0 + (\varrho_{N+1} - \varrho_0)\,\frac{\left(\frac{r}{l}\right)^m - 1}{\left(\frac{r}{l}\right)^{N+1} - 1}. \tag{65}$$

Starting with a density which is uniform in each cell and fulfills (65), the coarse-grained density ϱ_m is stationary, while the exact density $\varrho(x,p)$ inside the cells takes constant values in the horizontal (expanding) direction, and accumulates more and more structure in the vertical (contracting) one (cf. Figs. 10 and 11). In particular, after one iteration (Fig. 11 with $l_2 = r_2 = \tilde{r_2} = \tilde{l_2} = 0$, $\tilde{r}_1 = l_1 = l$, $\tilde{l}_1 = r_1 = r$, and $\tilde{s} = s$) one finds the uniform densities $l\varrho_{m+1}/r$, ϱ_m, and $r\varrho_{m-1}/l$, on three strips with heights br, bs and bl from bottom to top, respectively. In the following iteration, the density in any of these region is structured further in the vertical direction as shown in Fig. 12a. Subsequent iterations lead to a successive refining of the structure of the density such that it approaches asymptotically a self-affine measure [4, 17, 18]. Gaspard therefore suggested to consider instead the cumulative measure, which is in our model

$$R_m(p) = \int_0^a \mathrm{d}x \int_0^b \mathrm{d}p'\ \varrho(x,p'). \tag{66}$$

Its time evolution is shown in Fig. 12b. One easily verifies that this function fulfills the recursion relation

$$R_m(p) = \begin{cases} l & R_{m+1}\left(\frac{p}{r}\right) & \text{for} & 0 < \frac{p}{b} < r \\ s & R_m\left(\frac{p-br}{s}\right) + lR_{m+1}(b) & \text{for} & r < \frac{p}{b} < r+s \\ rR_{m-1}\left(\frac{p-b(r+s)}{l}\right) + lR_{m+1}(b) + sR_m(b) & & \text{for} & r+s < \frac{p}{b} < b\,. \end{cases} \tag{67}$$

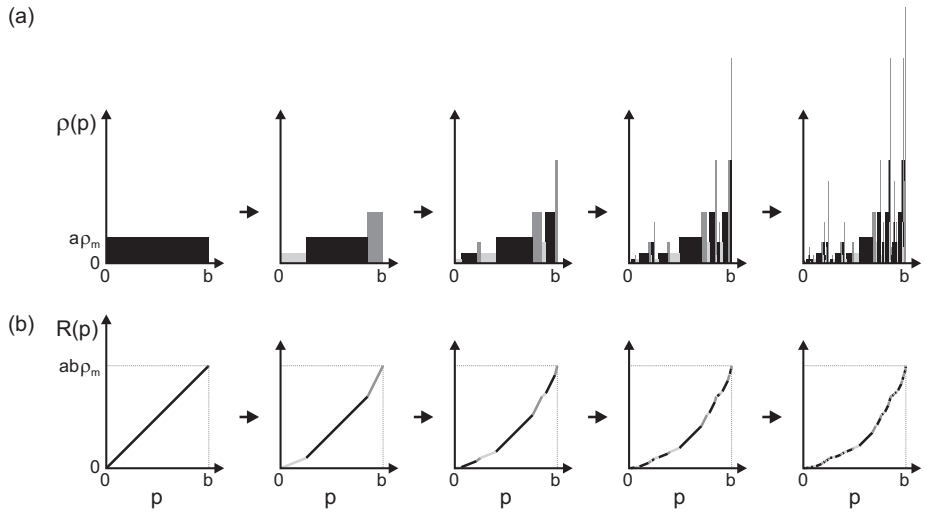

Figure 12: The invariant measure for cell m of a three-strip multibaker map with $l = 0.15$, $s = 0.60$ and $r = 0.25$ and with average densities $\varrho_{m-1} = \frac{6}{5}\varrho_m$ and $\varrho_{m+1} = \frac{2}{3}\varrho_m$ in cells $m\pm1$ fulfilling (44) with $p_{-2} = p_2 = 0$. (a) The first five levels of the hierarchical construction of the invariant measure along the vertical direction. It approaches a self-affine (multifractal) distribution. Regions entering in the first step of refinement from the right (left) are shaded in light (dark) grey. Subsequently, these colors are preserved. (b) The first five levels of the hierarchical construction of the cumulative measure which approaches a Takagi function [4, 5, 18]. The choice of shadings matches the one in part (a).

It rises strictly monotonously from 0 to $\Gamma\varrho_m$, and approaches a nowhere differentiable function in the limit of infinite refinement.

Gaspard based his argument regarding entropy production in the Hamiltonian multibaker map on the occurrence of these non-differentiabilities [4, 19]. He succeeded by this to derive the first local entropy balance for a deterministic dynamical system. His original argument shows that irreversible entropy production cannot be avoided in steady states of nonequilibrium systems characterized by fractal invariant measures. Strictly speaking, however, fractal measures are only encountered in the limit where the number of cells tends to infinity ($N \to \infty$), which cannot be taken in a physical system with a fixed gradient and cell size. Furthermore, thermodynamic entropy production is also expected in transient states where the densities are still (piecewise) smooth. A recent discussion of these questions can be found in Refs. [20, 29].

This apparent contradiction can be resolved by noting [23, 24] that the concept of a steady state in thermodynamics must not be confused with that of an invariant measure in a dynamical system. In fact, stationarity in thermody-

namics only requires the stationarity of the average densities in regions of small lateral extent, like for instance the unit cell of the lattice in the Lorentz gas, or correspondingly the cells of linear size a of the multibaker map. Structures in phase space below this *finite* scale are meaningless in thermodynamics. Their occurrence gives rise to entropy production. Thermodynamically meaningful results are expected to be found in the macroscopic limit, where the extent a of the cells is much smaller than the system size or typical length scales related to the variation of the coarse-grained densities. Due to the exponentially refining structures in chaotic systems, one expects in this limit to encounter structures on much finer scales than a, such that the results of a thermodynamic description taking into account this cutoff turn out to be robust against details of the prescription for coarse graining. In particular this approach faithfully predicts entropy production also in finite systems (provided $N \gg 1$) and in transients. In the following we concentrate on results obtained in this spirit.

5.2 Particle Transport and Entropy Balance in Isothermal Systems. The macroscopic description of transport considers the evolution of (thermodynamic) averages in regions of small spatial extension. In this spirit particle transport driven by an external field and a local density gradient is faithfully described by the multibaker map of the previous Section. We saw that the transport process is related to an advection diffusion equation on the macroscopic level, and that the irreversible entropy production is also consistent with the thermodynamic form. These results remain valid when the next-to-nearest-neighbor transition probabilities (r_2, l_2) vanish. One can show [22–24] that even a full entropy balance holds on the macroscopic level with

$$\Phi = -\nabla j^{(s)} + \Phi^{(\text{thermostat})} \tag{68}$$

as the entropy flux. Here

$$j^{(s)} = -j \left[1 + \ln \frac{\rho}{\rho^\star} \right] \tag{69}$$

is the entropy current in full consistency with thermodynamics. One finds, however, another contribution to the flux

$$\Phi^{(\text{thermostat})} = -\frac{vj}{D}, \tag{70}$$

which is not a divergence but is due to heat taken out *locally* by the thermostating procedure. Note that the full entropy balance is independent of the cell size in the macroscopic limit, implying that the results of Sect. 2, when applied locally, can become independent of the coarse-graining size in this limit. The appearance of a finite $\Phi^{(\text{thermostat})}$ is a deviation from traditional thermodynamics but its presence is unavoidable in an isothermal model. After all, such models are considered to mimic transport at a fixed temperature, such that they need

not have any temperature variable. A bulk system, however, is warmed up by the Joule heat such that the assumption of a uniform stationary temperature profile is not valid. To let the system approach such an isothermal steady state, one has to remove the Joule heat leading locally to the heat flux $\Phi^{(\text{thermostat})}$.

5.3 Green-Kubo Relation in the Isothermal Case. We consider long trajectories of length $t = n\tau$ which are consistent with a steady-state density distribution ϱ_m. The Green-Kubo relation for multibaker maps should then relate the diffusion coefficient D of their dynamics to the variance of the displacements Δn of the trajectory segments around the mean $a(r-l)n$. The variance of $a\Delta n - a(r-l)n$ is to be taken with the probability density $P_n(\Delta n, \mu)$ for finding a trajectory segment of length $t = n\tau$ centered at μ with displacement $a\Delta n$. For the multibaker this probability takes the form

$$P_n(\Delta n;\mu) = \frac{\varrho_{\mu-\Delta n/2}}{\sum_{m=1}^{N}\varrho_m} \sum_{\substack{n_l,\,n_s,\,n_r \\ n_r+n_s+n_l=n \\ n_r-n_l=\Delta n}} \mathcal{N}_t^{(\mu)}(n_l,n_r)\; l^{n_l} s^{n_s} r^{n_r}. \tag{71}$$

The first factor of (71) accounts for the probability that the trajectory segment starts in cell $m_0 = \mu - \Delta n/2$. The other factor is the probability to find a segment with displacement Δn, where $\mathcal{N}_t^{(\mu)}(n_l, n_r)$ denotes the number of trajectories which are centered at μ, make n_l (n_r) steps to the left (right), and never leave the chain. Consistently with the piecewise-linear character of the multibaker dynamics, these probabilities are taken to be independent. In particular, $\mathcal{N}_t^{(\mu)}(n_l, n_r) = n!/(n_l!\, n_s!\, n_r!)$ if the considered trajectories stay inside the chain, which we will assume in the following.[3]

Using that $\Delta n = n_r - n_l$, and that Δn can take any value between $-n$ and n, we have

$$\begin{aligned}\left\langle a^2(\Delta n-(r-l)n)^2\right\rangle &= \sum_{\mu}\sum_{\Delta n=-n}^{n}[n_r-n_l-(r-l)n]^2\; P_n(\Delta n,\mu)\\ &= \frac{a^2}{\sum_m \varrho_m}\sum_{\mu}\varrho_{\mu-\Delta n/2}\\ &\times \sum_{\substack{n_l,\,n_s,\,n_r\\ n_r+n_s+n_l=n}}[n_r-n_l-(r-l)n]^2\frac{n!}{n_l!\,n_s!\,n_r!}\; l^{n_l}s^{n_s}r^{n_r}.\end{aligned} \tag{72}$$

Note that the density dependent factor cancels, and what is left is exactly the same expression as for random walks. Thus,

[3] This assumptions implies that the length of the system is sufficiently large such that the escape of trajectories from the chain can be neglected.

$$\left\langle a^2(\Delta n - (r-l)n)^2 \right\rangle = 2Dn\tau \tag{73}$$

with $D = a^2(r+l)/(2\tau)$.

We can then express the diffusion coefficient as

$$D = \frac{a^2}{2n\tau} \sum_{i=1}^{n} \sum_{j=1-i}^{n-i} \left\langle [m_i - m_{i-1} - (r-l)][m_{i+j} - m_{i+j-1} - (r-l)] \right\rangle. \tag{74}$$

Here m_i stands for the index of the cell the trajectory visited at time $i\tau$ such that $\Delta n \equiv m_n - m_0 = \sum_{i=1}^{n} m_i - m_{i-1}$. Taking into account that in a steady state the average is expected to depend only on j due to time translation invariance, and that n is large, one obtains

$$\begin{aligned} D &\approx \frac{a^2}{2\tau} \sum_{j=-\infty}^{\infty} \langle [m_1 - m_0 - (r-l)][m_{j+1} - m_j - (r-l)] \rangle \\ &\equiv \frac{\tau}{2} \sum_{j=-\infty}^{\infty} \langle (v_0 - v)(v_j - v) \rangle \,. \end{aligned} \tag{75}$$

Here $v = a(r-l)/\tau$ stands for the the drift velocity, and we have introduced the instantaneous velocities

$$v_i \equiv \frac{a}{\tau}(m_{i+1} - m_i) \tag{76}$$

which can take on the values $\pm a/\tau$ or zero. Eq. (75) constitutes thus a discrete version of the Green-Kubo relation.

In the macroscopic limit $\tau \to 0$, the sum can be approximated by an integral, and we find the common expression of the Green-Kubo relation

$$D = \frac{1}{2} \int_{-\infty}^{\infty} \mathrm{d}t \, \left\langle [v(0) - v][v(t) - v] \right\rangle. \tag{77}$$

5.4 Energy Transport. In order to gain further insight into the role of heat and entropy fluxes in deterministic models for transport [65, 66], we introduce (cf. [30–32]) a new field ϱT, which plays the role of a kinetic-energy density. This field is also driven by the baker dynamics, but with a time evolution adapted according to physical intuition. In contrast to the number of particles, the kinetic energy per unit volume $\varrho_m T_m$ is not a conserved quantity. Its new values $\varrho'_{m,j} T'_{m,j}$ on the strips $j = L, S, R$ (cf. Figs. 10,11) contain in our model a contribution from the particle flow and, in addition, also a source term of strength q_m (corresponding to local heating) per unit time, which is constant in every cell:

$$\begin{aligned} \varrho'_{m,r}\, T'_{m,r} &= \frac{r}{l}\, \varrho_{m-1}\, T_{m-1}\, \left[1 + \tau q_m\right], \\ \varrho'_{m,s} T'_{m,s} &= \varrho_m\, T_m \left[1 + \tau q_m\right], \\ \varrho'_{m,l}\, T'_{m,l} &= \frac{l}{r}\, \varrho_{m+1}\, T_{m+1} \left[1 + \tau q_m\right]. \end{aligned} \tag{78}$$

There is a unique choice for q_m where the time evolution of the kinetic energy becomes consistent with thermodynamics in the macroscopic limit (cf. below). In other cases the source term leads to a non-vanishing entropy flux $\Phi^{(\text{thermostat})}$, and can be considered to characterize the *thermostating procedure* applied.

An update of the average kinetic energy can be calculated similarly to the update of the density. In cell m the average value $\varrho'_m T'_m$ after one time step is obtained by averaging the different contributions Eq. (78) on the strips, yielding

$$\varrho_m^{'} T_m^{'} = [\varrho_m T_m (1 - r - l) + r \varrho_{m-1} T_{m-1} + l \varrho_{m+1} T_{m+1}] \, [1 + \tau q_m]. \tag{79}$$

For a fixed set of transition probabilities r, l and the choice $q_m = 0$, Eq. (79) implies a passive advection of the T field by the deterministic (x, p) dynamics. The presence of the source terms q_m makes the advection non-passive. The quantity T_m is considered to represent the (kinetic) temperature of cell m.

In the macroscopic limit the particle current is still

$$j = \rho v - D \partial_x \rho, \tag{80}$$

where v is the drift due to an external field, and for the temperature equation we find:

$$\partial_t T = qT + \frac{\partial_x (\rho \, D \, \partial_x T)}{\rho} - j \frac{\partial_x T}{\rho}. \tag{81}$$

This clearly shows that the source distribution $q(x)$ [the macroscopic limit of q_m] influences the temperature profile, and different choices of $q(x)$ can lead to different steady states. In particular, states with spatially and temporally constant T, as they are commonly considered in nonequilibrium molecular dynamics simulations based on deterministic thermostats, require an identically vanishing q.

5.5 The Entropy Balance in the Presence of Temperature Gradients. In the presence of a non-uniform spatial temperature profile, we adopt a temperature dependent reference density $\varrho^\star(T) \equiv T^\gamma$, in close analogy with a classical ideal gas law. Here γ is a free parameter. The entropy S_m of cell m is

$$S_m = -a \varrho_m \ln \frac{\varrho_m}{\varrho^\star(T)}. \tag{82}$$

A calculation similar to the one carried out in Sects. 4.1 and 4.4 yields for the irreversible entropy production in the macroscopic limit [30, 31]

$$\sigma^{(\text{irr})} = \frac{j^2}{\rho D} + \gamma \rho D \left[\frac{\partial_x T}{T} \right]^2, \tag{83}$$

in full harmony with the results of Irreversible Thermodynamics [2, 67]. The coefficient in front of the term $(\partial_x T/T)^2$ due to temperature gradients is thus

be identified with the heat conductivity λ, i.e., $\lambda = \gamma\rho D$. The entropy current can be expressed as

$$j^{(s)} = -A\, j - \lambda\, \partial_x T/T, \tag{84a}$$

with

$$A \equiv \left[1 + \ln\left(\varrho T^{-\gamma}\right)\right]. \tag{84b}$$

For the flux into the thermostat we obtain

$$\Phi^{(\text{thermostat})} = \gamma\rho q - vj/D. \tag{85}$$

It is the difference of a term proportional to the source q, and a term corresponding to the change of entropy associated with Joule heating vj/D due to the drift v of the particles. In thermodynamics of bulk systems $\Phi^{(\text{thermostat})} = 0$, and the source term q takes the form

$$q^* = vj/\lambda. \tag{86}$$

All dissipative heat is then carried by the heat current to the boundaries of the system. This can only be achieved if there is a temperature dynamics in the system, and shows that a non-vanishing $\Phi^{(\text{thermostat})}$ is unavoidable when modeling drift in a system with spatially and temporally constant temperature.

5.6 Thermoelectric Cross Effects. Cross effects appear in Irreversible Thermodynamics if at least two independent driving forces contribute to the basic currents. Our multibaker with the kinetic-energy field faithfully describes thermoelectric cross effects, where, besides the external field or density gradient, also the temperature gradient contributes to the particle current. Vice-versa, the density gradient also gives rise to a heat current in addition to the one generated by the field or the density gradient.

In thermodynamics the particle current is of the form

$$j = \rho v - \frac{\sigma_{el}}{e^2}(\partial_x \mu_c + e\alpha\partial_x T), \tag{87}$$

where μ_c denotes the chemical potential of the particles, and v is the drift velocity due to an external electric field E, which is related to the conductivity σ_{el} by

$$v = \frac{\sigma_{el} E}{e\rho}. \tag{88}$$

The coefficient α in (87) is the thermoelectric power (or Seebeck coefficient).

It is easy to see that the multibaker result (80) for the macroscopic particle current is consistent with (87). As indicated by (82), the equation of state of the 'multibaker gas' is that of a classical ideal gas with γ as its (constant volume)

specific heat measured in units of Boltzmann's constant. Therefore the chemical potential as a function of the density and temperature should be

$$\mu_c = T(1+\gamma) + T\ln\left(\rho T^{-\gamma}\right). \tag{89}$$

Hence, we can express the gradient of the chemical potential with that of the density and the temperature as

$$\partial_x \mu_c = \frac{T}{\rho}\partial_x \varrho + [1 + \ln\left(\rho T^{-\gamma}\right)]\partial_x T. \tag{90}$$

Substituting this into (87) we see that it is equivalent with (80) provided that

$$D = \frac{\sigma_{el} T}{e^2 \rho}, \tag{91a}$$

and

$$\alpha = -\frac{1}{e}[1 + \ln\left(\rho T^{-\gamma}\right)]. \tag{91b}$$

The first condition is Einstein's relation which is expected to be valid in a weakly interacting classical gas, and the second one is an expression of the Seebeck coefficient with local thermodynamic state variables.

The thermodynamic form of the entropy current [2] in the presence of both temperature differences and an external field or density gradient is

$$j^{(s)} = -\frac{e\Pi}{T} j - \lambda\, \partial_x T/T, \tag{92}$$

with Π as the Peltier coefficient. A comparison with the multibaker results (84a) and (84b) immediately yields the Peltier coefficient in the form of

$$\Pi = -\frac{T}{e}\left[1 + \ln\left(\rho T^{-\gamma}\right)\right]. \tag{93}$$

This implies that

$$\Pi = \alpha T \tag{94}$$

which is nothing but Onsager's reciprocity relation for thermoelectric effects. By this we have expressed all the kinetic coefficients σ_{el}, λ, α and Π with system parameters.

The forms (87) and (92) of the currents express the presence of cross effects. The measurement of the (off-diagonal) Onsager coefficients is however not possible in homogeneous systems. It requires a junction between two materials [68]. In analogy with typical experimental arrangements, this situation can also be modeled in the framework of multibakers by considering two chains with

different transition probabilities (i.e., different "material properties"), which are joined together [32].

Momentum and heat transport in viscous flows. Recently, also a consistent description of shear flow, the accompanied viscous heating, and the corresponding entropy balance has been given in the framework of a multibaker [71]. The problem of the laminar motion of an incompressible viscous fluid sheared by the relative motion of two parallel walls has been treated. In this case the multibaker dynamics is area preserving and drives two fields: the velocity and the temperature distributions. In the macroscopic limit, in which the kinematic viscosity is kept finite, the transport equations go over into the Navier-Stokes and the heat-conduction equation of viscous flows sheared in a given direction. Simultaneously, the entropy balance equation for this multibaker converges to the well known thermodynamical form. The inclusion of an artificial heat sink can stabilize steady states with constant temperatures. This mimics again a thermostating algorithm used in nonequilibrium-molecular dynamics simulations.

5.7 The Irreversible Entropy Production as the Average Growth Rate of the Relative Phase-Space Density in Steady States. In steady states of open systems with density gradients, the rate of irreversible entropy production $\sigma^{(irr)}/\varrho$ per particle is the (weighted) average of the growth rate σ_ϱ of the relative local phase-space density $\varrho_t(x,p)/\varrho^*(x,p)$

$$\sigma_\varrho(x,p) \equiv \frac{1}{\tau}\,\ln\frac{\varrho_\tau(x,p)/\varrho^\star(x,p)}{\varrho_0(x,p)/\varrho^\star(x,p)}, \tag{95}$$

where τ is the time unit and $\varrho^\star$ accounts for the temperature dependence of the normalization of the density introduced in Eq. (82). This can be seen by using Eq. (46) to work out (48) for the non-isothermal case, and setting $\varrho_0(x,p) = \varrho_m$ and $\varrho_\tau(x,p) = \varrho'_{m,i}$. This *local* expression holds irrespective of boundary conditions. In general, it is different from zero even in macroscopically steady states (when the coarse-grained density and other coarse-grained averages are time-independent) because of the never stopping time evolution of the phase-space density ϱ. Besides phase-space contraction, σ_ϱ also characterizes the mixing of regions with different macroscopic densities. Hence, it does not vanish in boundary-driven, volume-preserving systems. Only in macroscopically homogeneous steady states $\sigma_\varrho(x,p)$ reduces to the local phase-space contraction rate $\sigma(x,p)$ so that entropy production and phase-space contraction can be identified in such cases only.

In a steady state of a non-isothermal system the generalized form of the entropy production (48) can be interpreted as a weighted sum of the logarithm of ratios $\varrho'_{m,i}{T'_{m,i}}^{-\gamma}/(\varrho'_m {T'_m}^{-\gamma})$. This suggests as an alternative view to consider the steady-state entropy production as the sum of contributions due to steps along trajectories, which contribute

$$\begin{aligned}
&\frac{1}{\tau}\ln\left[\frac{r_m\varrho_m T_m^{-\gamma}}{l_{m+1}\varrho_{m+1}T_{m+1}^{-\gamma}(1+\tau q_{m+1})^{-\gamma}}\right] \quad \text{for a step from cell } m \text{ to } m+1,\\
&\qquad\frac{\gamma}{\tau}\ln\left[1+\tau q_m\right] \qquad \text{whenever it stays in cell } m, \qquad (96)\\
&\frac{1}{\tau}\ln\left[\frac{l_m\varrho_m T_m^{-\gamma}}{r_{m-1}\varrho_{m-1}T_{m-1}^{-\gamma}(1+\tau q_{m-1})^{-\gamma}}\right] \quad \text{for a step from cell } m \text{ to } m-1.
\end{aligned}$$

The density ratios enter Eq. (96) because of the mixing in cell m of different coarse-grained densities coming from the neighboring cells $m-1, m+1$. The factors $1+\tau q_m$ stem from the time-dependence of the average local kinetic energy (i.e., of the temperature) as described by (78).

Due to the appearing of the source terms in Eq. (96), the sum of contribution to the entropy production cannot be evaluated in general. For a thermostated system, however, where $q_m = 0$, the single-step contributions (96) add up like a telescoping sum along a trajectory, and the entropy production changes sign when following a trajectory backward in time. Consequently, the local irreversible entropy production averaged over trajectories of length n, which make n_l (n_r) steps to the left (right) and are centered at the half-integer cell index μ, i.e., which start in cell $m_0 = \mu - \Delta n/2$ and end in $\mu + \Delta n/2$, where $\Delta n \equiv n_r - n_l$, is

$$\sigma_\varrho^{(\mu)}(n_l, n_r) = \frac{1}{n\tau}\ln\left[\left(\frac{r}{l}\right)^{\Delta n}\frac{\varrho_{\mu-\Delta n/2}}{\varrho_{\mu+\Delta n/2}}\left(\frac{T_{\mu-\Delta n/2}}{T_{\mu+\Delta n/2}}\right)^{-\gamma}\right]. \qquad (97)$$

It is independent of the details of the sequence of steps. The macroscopic limit of (97) is $\sigma^{(irr)}$ of (83) divided by the density ρ.

5.8 Fluctuation Theorem for Entropy Production in Steady States with Density Gradients. In this subsection we derive a large-deviation theorem for entropy production fluctuations of multibakers. First, we restrict to this end to systems with a spatially constant, stationary temperature (i.e., $T_m = T$ for all cells and q_m vanishes identically). According to Eq. (97), the rate $\sigma_\varrho^{(\mu)}(n_l, n_r)$ then only depends on n_l and n_r through Δn. Hence, the probability $\Pi_t^{(\mu)}(\sigma_\varrho)$ of finding a value $\sigma_\varrho \equiv \sigma_\varrho^{(\mu)}(\Delta n)$ along a trajectory segments of length $t = n\tau$ centered at μ is the same as the probability $P_n(\Delta n; \mu)$ [Eq. (71)] for finding a trajectory segments of length $t = n\tau$ centered at μ with displacement $a\Delta n$:

$$\Pi_t^{(\mu)}\left(\sigma_\varrho^{(\mu)}(\Delta n)\right) = P_n(\Delta n; \mu). \qquad (98)$$

We recall that $\mathcal{N}_t^{(\mu)}(n_l, n_r)$ denotes the number of trajectories which make n_l (n_r) steps to the left (right), and never leave the chain. Comparing trajectories with their time-reversed counterparts, we find that $\mathcal{N}_t^{(\mu)}(n_l, n_r) = \mathcal{N}_t^{(\mu)}(n_r, n_l)$.

Moreover, time-reversed trajectory segments produce the same entropy up to a change of sign, $\sigma_\varrho^{(\mu)}(\Delta n) = -\sigma_\varrho^{(\mu)}(-\Delta n)$. Thus,

$$\frac{\Pi_t^{(\mu)}\left(\sigma_\varrho^{(\mu)}(\Delta n)\right)}{\Pi_t^{(\mu)}\left(\sigma_\varrho^{(\mu)}(-\Delta n)\right)} = \frac{\varrho_{\mu-\Delta n/2} \sum\limits_{\substack{n_l,n_s,n_r \\ n_r+n_s+n_l=n \\ n_r-n_l=\Delta n}} \mathcal{N}_t^{(\mu)}(n_l,n_r)\, l^{n_l} s^{n_s} r^{n_r}}{\varrho_{\mu+\Delta n/2} \sum\limits_{\substack{n_l,n_s,n_r \\ n_r+n_s+n_l=n \\ n_r-n_l=\Delta n}} \mathcal{N}_t^{(\mu)}(n_l,n_r)\, l^{n_r} s^{n_s} r^{n_l}}$$

$$= \frac{\varrho_{\mu-\Delta n/2}}{\varrho_{\mu+\Delta n/2}} \left(\frac{r}{l}\right)^{\Delta n} = \exp\left[n\tau\, \sigma_\varrho^{(\mu)}(\Delta n)\right], \tag{99}$$

where we used in the last step that T is constant. After taking the logarithm of both sides, the right-hand side is exactly $t = n\tau$ times $\sigma_\varrho^{(\mu)}(\Delta n)$. Eq. (99) constitutes therefore a *local* fluctuation theorem [27]

$$\frac{1}{t}\, \ln \frac{\Pi_t^{(\mu)}\left(\sigma_\varrho^{(\mu)}(\Delta n)\right)}{\Pi_t^{(\mu)}\left(\sigma_\varrho^{(\mu)}(-\Delta n)\right)} = \sigma_\varrho^{(\mu)}(\Delta n). \tag{100}$$

It applies to trajectories of given center μ and of finite length $t = n\tau$, and states that the logarithm of the ratio of the probabilities to find local entropy production rates $\sigma_\varrho^{(\mu)}$ and $-\sigma_\varrho^{(\mu)}$ over a time span t is the same as the total entropy production $t\sigma_\varrho^{(\mu)}$ over this time interval.

In order to obtain also a *global* fluctuation theorem one needs the probability $\Pi_t(\sigma_\varrho)$ of finding a value σ_ϱ irrespective of the position of the trajectory. This is obtained by summing up the contributions of all $\Pi_t^{(\mu)}(\sigma_\varrho)$, $\mu = 1, \frac{3}{2}, 2, \frac{5}{2}, \cdots N$, and observing that μ contributes to $\Pi_t(\sigma_\varrho)$ if and only if there is a displacement Δn_μ with $\sigma_\varrho = \sigma_\varrho^{(\mu)}(\Delta n_\mu)$. Consequently,

$$\Pi_t(\sigma_\varrho) = \sum_\mu \Pi_t^{(\mu)}\left(\sigma_\varrho^{(\mu)}(\Delta n_\mu)\right)$$

$$= \sum_\mu \frac{\varrho_{\mu-\Delta n_\mu/2}}{\varrho_{\mu+\Delta n_\mu/2}} \left(\frac{r}{l}\right)^{\Delta n_\mu} \Pi_t^{(\mu)}\left(\sigma_\varrho^{(\mu)}(-\Delta n_\mu)\right)$$

$$= \exp\left(t\sigma_\varrho\right)\, \Pi_t(-\sigma_\varrho), \tag{101}$$

where we used Eqs. (97,99) with Δn_μ to obtain the second equality.

This means that

$$\frac{1}{t} \ln\left[\frac{\Pi_t(\sigma_\varrho)}{\Pi_t(-\sigma_\varrho)}\right] = \sigma_\varrho \tag{102}$$

holds for the steady state ϱ_m of the time-reversible system. It is worth emphasizing that the result does not depend on the particular choice of boundary conditions. It generalizes the Gallavotti-Cohen fluctuation theorem [49, 51] to steady states which need no longer be homogeneous in density.

The calculation can be extended even to a class of steady states with non-trivial temperature profiles stabilized by thermostating consistent with $q_m = 0$. Assuming that the number of trajectory segments starting in cell $m_0 = \mu - \Delta n/2$ is proportional to $\varrho_{m_0} T_{m_0}^{-\gamma}$, and using the corresponding modification of Eq. (71), one can recover the fluctuation relation (102) also for non-isothermal cases. With the original form of (71) on the other hand, the right hand side of (102) is modified such that a temperature dependent term appears besides σ_ϱ which removes the contribution of the heat current to σ_ϱ. This indicates that the structure of fluctuation relations is more delicate in the presence of temperature gradients than in isothermal cases, even with thermostating. Under which conditions fluctuation relations hold in non-thermostated systems, and which form they take in the presence of steady temperature gradients is an open question at present.

§6. Discussion

We take up a few general issues here, which further illuminate the relation between the modeling of transport by multibaker maps and other approaches pursued in the literature [and in the other contributions to the present volume].

6.1 Deviations from Dynamical Systems Theory. The multibaker approach deviates in several features from those based on dynamical systems. The most essential one is the openness of the system, i.e., the consequences of using non-trivial boundary conditions. These are prescribed for the fields ϱ and T specifying the thermodynamic state, and *not* for the (x, p) dynamics. The physical motivation of this is that we consider the multibaker map as a model for the dynamics in the single-particle phase space of a weakly interacting many-particle system. In the spirit of kinetic theory, the state of the many-particle problem is described by a *distribution function* in this phase space. If one is not intending to model the reservoirs, this distribution function is subjected to boundary conditions. It is this feature which leads (after averaging) to macroscopic transport or hydrodynamic equations subjected to non-trivial boundary conditions. We feel that it is unavoidable to go beyond the scope of dynamical system theory in this point, in order to obtain a closer analogy with transport phenomena. Multibaker models seem to represent the weakest necessary generalization. They still allow us to use well-established tools of dynamical-systems theory. For instance, the Frobenius-Perron equation of the map $\mathcal{B}(x, p)$, which describes the time evolution of the phase-space density $\varrho(x, p)$ for x values in the multibaker chain, takes the traditional form except for an augmentation

with the boundary conditions at the two ends. A slightly modified version of the Frobenius-Perron equation also takes into account the local source term, and can then be applied to the kinetic-energy density ϱT [31]. The invariant measures are forced on the systems by the boundary conditions and they differ from the natural (SRB) measures encountered in the presence of periodic boundary conditions.

Another deviation from dynamical-system approaches is the possibility of local investigations. Since spatial variance is ubiquitous even in the coarse-grained fields of multibakers, it is worth concentrating on cell quantities. By this approach one can establish an analogy with the local transport equations and the local entropy balance. Local investigations can be carried out in periodic multi-cell models, too [32]. In order to see sustained inhomogeneities of the fields, one considers in that case a multibaker chain driven by a strongly biased dynamics in a very small region of the chain. The steady-state field distributions are determined by the difference of the bias in this region to the one in the remainder of the system. In steady states these models are equivalent with open multibakers [32]. However, they differ in transient cases due to the correlation of the dynamics in the vicinity of the two "ends" of periodic systems. Open multibaker models are therefore at present the only analytically accessible tool to comprehensively study transport processes driven by externally prescribed boundary conditions.

6.2 Interpretation of Coarse Graining. Coarse graining plays an essential role in different branches of physics. Even the theory of classical, equilibrium statistical mechanics described by closed volume-preserving models, relies on this concept [45]. After all, the concept of the number of states or of the partition sum requires partitioning the phase space into small boxes. Before the rise of quantum mechanics this partitioning was arbitrary, but later the Correspondence Principle together with Heisenberg's uncertainty relation fixed the size of partitioning. It amounts to the smallest product of the location and momentum uncertainty $\Delta x\, \Delta p = h$, where h is Planck's constant. In the notation of Sect. 2 of the present paper, this means that the dimensionless linear size of the boxes for coarse graining is $\varepsilon \sim h^{1/2}$. Since the size is given by a universal constant, in equilibrium statistical mechanics we do not think of changing the box size. It is illuminating to recognize, however, that there is this dependence. In fact, the well known relation $S(E) = \ln\left(\Gamma(E)/h^{3N}\right)$ between equilibrium entropy S and the phase-space volume $\Gamma(E)$ at fixed energy E in a closed system of N particles each moving in three dimensions implies that $S(E)$ depends logarithmically on h. The coarse-grained entropy $S_{\varepsilon=h^{1/2}}(t)$ converges to the value of $S(E)$ [69, 70]. By a formal change of h to h' we find a shift by $-3N \ln(h'/h)$ corresponding to the fact that the phase space is $d = D_I = 6N$ dimensional. The coarse graining discussed in Sect. 2 for general dynamical systems is similar in spirit since it is based on coarse graining with the finest possible resolution in phase space.

The concept of coarse graining in Irreversible Thermodynamics is markedly different since it is used to define local thermodynamic variables. This is done

by dividing the real space into boxes of linear size much smaller than the total size of the system, so that the box is large enough to contain a yet macroscopic number of particles. The coarse-grained fields are then the thermodynamic state variables of the box in accordance with the hypothesis of local equilibrium. They are obtained by integrating out all momentum-like variables and averaging over the box in real space. The linear size a of the multibaker map is the analog of the box size. Due to the integration over p, the transport and the entropy flow is along the x direction — a feature which is not present in the general dynamical system approach. It is within this setting that the weak resolution dependence of the entropy can fully be removed after taking the appropriate macroscopic limit. Only in this limit one can hope for a full analogy with thermodynamic relations. Whether it is indeed found might depend on system parameters. For instance, a non time-reversible dynamics never leads to results consistent with thermodynamics.

6.3 Interpretation of the Macroscopic Limit. The macroscopic limit, which we briefly denote as $a, \tau \to 0$, is to be understood as the limit with a clear separation of length and time scales between the dynamical and macroscopic degrees of freedom. More precisely, we consider systems of linear extension L much larger than the cell size a, and observe the fields on the macroscopic diffusion time scale L^2/D or on the drift time scale D/v^2. In this case the dimensionless cell size a/L and time unit $\tau D/L^2$ (or $\tau v^2/D$) are much smaller than unity. The notation $a, \tau \to 0$ should be interpreted as the commonly used phenomenological continuum limit of hydrodynamic theories. It is meaningless to literally let the cell size a to vanish, since the local averages and the concept of local equilibrium would then become meaningless. As mentioned at the end of Section 3.1, the cell size and the time unit are related by the momentum p of particles. Therefore, when modeling the Lorentz gas, the limits $a \to 0$ and $\tau \to 0$ should be carried out under observation of the additional condition that the momentum, i.e., the ratio a/τ is fixed.

The results obtained in the macroscopic limit are structurally stable. Carrying out coarse graining not only over one cell, but over any finite number m_c of cells or after every n time units rather than after just one, one finds a dependence of the relaxation time on m_c and n. Taking the macroscopic limit with fixed m_c or n, however, means that the size of the coarse-graining region or the typical time after which coarse graining is applied is still much smaller than their macroscopic counterparts. Therefore, in the macroscopic limit the resulting transport equations become independent of m_c and n. Consequently, the physically relevant relaxation times do not depend on these details of the prescription for coarse graining. Rather they are related to the spectrum of the time-evolution operator of the thermodynamic densities, *i.e.*, they are independent of the time t_ε discussed in Sect. 2. The latter time characterizes the emergence of fractal structures on the scale of ε in the (thermodynamically not immediately relevant) exact densities.

6.4 Outlook and Open Problems. The modeling of transport by simple (i.e., analytically accessible) dynamical systems is presently a fruitful and rapidly expanding enterprise. Naturally, however, there is a number of open problems still waiting for their solution

- In our approach the fields ϱ and T are considered as independent distribution functions in the single-particle phase space of a many-particle problem. After all, there is no momentum conjugated to the spatial variable of multibaker maps which would relate the kinetic-energy density to the density. A closer comparison with particle dynamics would therefore be useful.
- Weak interactions are needed in order to induce relaxations keeping up the local thermodynamic equilibrium in any small region in space. It would be interesting to implement their role explicitly in order to clarify the role they play for, e.g., the occurrence of the source term in the heat equation.
- A general reversible dynamics for heat is missing. It is unclear how (or even whether) the source terms in the kinetic energy density can be implemented reversibly.
- The role of quantum-mechanical coarse graining in Irreversible Thermodynamics is open. At present there is not even a model in sight to address this question.

The multibaker approach can be considered as a search for the simplest mathematical structures which allow for a consistent description of transport phenomena. It is remarkable in how far consistency with Irreversible Thermodynamics can be obtained even without referring to relations naturally used in kinetic theory, like for instance the relation between momentum and kinetic energy. We are looking forward to explore other simple models to shed light on the open questions in the field.

Acknowledgements. Illuminating discussions with E.G.D. Cohen, J.R. Dorfmann, D. Evans, P. Gaspard, J. Krug, G.P. Morriss, G. Nicolis and Z. Rácz are gratefully acknowledged. We thank W. Breymann, L. Mátyás, and L. Rondoni for enjoyable and fruitful collaborations, and gratefully acknowledge support from the Hungarian Science Foundation (OTKA T17493, T19483, T032423).

A. Trajectories of the Thermostated Lorentz Gas

The kinetic energy of closed particle systems subjected to an external field grows quadratically in time. In order to avoid this undesired behavior in classical transport, such models are commonly coupled to noise terms [64] or to deterministic

thermostats [3]. The latter approach leads to deterministic equations of motion, which are however no longer volume-preserving (i.e., in particular they cannot be Hamiltonian). Here we explicitly solve these equations to obtain the trajectory of a single particle of charge e and mass m in the (x, y)-plane of the Lorentz gas, when it is subjected to an external field $\mathbf{E}$ and a deterministic thermostat fixing its kinetic energy. The Newton equations are in that case

$$\dot{\mathbf{q}} = \frac{\mathbf{p}}{m}, \tag{104}$$

$$\dot{\mathbf{p}} = e\mathbf{E} - \zeta\mathbf{p}, \tag{105}$$

where $\mathbf{q} \equiv (x, y)$ and $\mathbf{p} \equiv (p_x, p_y)$, are the position and the momentum of the particle, respectively. The dynamical friction coefficient ζ represents the action of the thermostat. It is fixed by the condition $\partial_t p^2 = 0$ that the kinetic energy of the particle is constant in time, leading to

$$\zeta = \frac{e\mathbf{E} \cdot \mathbf{p}}{p^2}. \tag{106}$$

Since the modulus of $\mathbf{p}$ is constant, one conveniently parameterizes the momentum by its angle with the y axis

$$\mathbf{p} = p\ (-\sin\theta, \cos\theta). \tag{107}$$

A.1 Time Reversibility and Phase-Space Contraction. For the choice (106) of ζ, the equations of motion (103) are invariant under reversing the direction of $\mathbf{p}$ and changing the sign of the time. Hence, the operation $\theta \mapsto \theta + \pi$ is an involution, which generates the time reversal also in the case of the thermostated Lorentz gas. As a consequence, the flow in the phase space $(\mathbf{q}, \mathbf{p})$ is still one-to-one, but it is no longer area preserving in the presence of the field. In that case the phase-space volume Γ changes with the rate

$$\partial_t \ln \Gamma \equiv \partial_q \dot{q} + \partial_p \dot{p} = -\zeta. \tag{108}$$

This rate has no definite sign. The net phase-space contraction $\sigma(t)$ along a trajectory segment from (x_0, y_0) at time $t = 0$ to (x, y) at time t is proportional to the displacement in the direction of the field. Taking (without restriction of generality) $\mathbf{E} = (E, 0)$, one finds that

$$\sigma(t) = \int_0^t \mathrm{d}t\ \zeta = \frac{meE}{p^2} \int_0^t \mathrm{d}t\ \dot{x} = \frac{meE}{p^2}(x - x_0). \tag{109}$$

A.2 The Form of Trajectories. We denote the initial direction of the trajectory by θ_0. After inserting Eq. (107) into Eq. (105) one then finds

$$\dot{\theta} = -\frac{eE}{p}\ \cos\theta. \tag{110}$$

With this input Eq. (104) can be integrated to yield

$$y - y_0 = -\frac{p^2}{meE} \int_{\theta_0}^{\theta} \mathrm{d}\theta = -\frac{p^2}{meE} (\theta - \theta_0), \tag{112}$$

$$x - x_0 = \frac{p^2}{meE} \int_{\theta_0}^{\theta} \mathrm{d}\theta \ \tan\theta = -\frac{p^2}{meE} \ \ln\left[\frac{\cos\theta}{\cos\theta_0}\right]. \tag{113}$$

Eliminating θ from these relations and setting $m = e = 1$ one finally recovers (34).

References

[1] H. B. Callen, Thermodynamics (Wiley, New York, 1960).
[2] S.R. de Groot, and P. Mazur, Nonequilibrium Thermodynamics (Elsevier, Amsterdam, 1962); (reprinted: Dover Publications, New-York, 1984).
[3] D.J. Evans and G.P. Morriss, Statistical Mechanics of Nonequilibrium Liquids (Academic Press, London, 1990); W.G. Hoover, Computational Statistical Mechanics (Elsevier, Amsterdam, 1991).
[4] P. Gaspard, Scattering, Chaos, and Nonequilibrium Statistical Physics (Cambridge Univ. Press, Cambridge, 1999).
[5] J.R. Dorfman, From molecular chaos to dynamical chaos, (Cambridge Univ.-Press, Cambridge, 1999).
[6] W.G. Hoover, Time Reversibility, Computer Simulation, and Chaos (World Scientific, Singapore. 1999).
[7] N.I. Chernov, G.L. Eyink, J.L. Lebowitz, Ya.G.Sinai, Phys. Rev. Lett. **70**, 2209 (1993); Comm. Math. Phys. **154**, 569 (1993).
[8] D. Ruelle, J. Stat. Phys. **85**, 1 (1996).
[9] E.G.D. Cohen and L. Rondoni, CHAOS **8**, 357 (1998).
[10] H.H. Diebner and O.E. Rössler, Z. Naturforsch. **53a**, 51 (1998).
[11] P. Gaspard and G. Nicolis, Phys. Rev. Lett. **65**, 1693 (1990).
[12] P. Gaspard and F. Baras, Phys. Rev. E **51**, 5332 (1995); P. Gaspard and J.R. Dorfman, Phys. Rev. E **51**, 28 (1995); E **52**, 3525 (1995).
[13] T. Tél, J. Vollmer, and W. Breymann, Europhys. Lett. **35**, 659 (1996).
[14] Z. Kaufmann, Phys. Rev. E **59**, 6552 (1999); Z. Kaufmann, A. Németh and P. Szépfalusy, Critical States of transient chaos, Phys. Rev. E **61**, 2543 (2000); Z. Kaufmann and P. Szépfalusy, Transient Chaos and Critical States in Generalized Baker Maps to appear in J. Stat. Phys., October 2000.
[15] W. Breymann, T. Tél, and J. Vollmer, Phys. Rev. Lett. **77**, 2945 (1996).
[16] G. Nicolis, D. Daems, J. Chem. Phys. **1000**, 19187 (1996); CHAOS **8**, 311 (1998); D. Daems, G. Nicolis, Phys. Rev. E **59**, 4000 (1999).
[17] P. Gaspard, J. Stat. Phys. **68**, 673 (1992).
[18] S. Tasaki and P. Gaspard, J. Stat. Phys. **81**, 935 (1995); S. Tasaki, T. Gilbert, and J.R. Dorfman, CHAOS **8**, 424 (1998).
[19] P. Gaspard, Physica A 240, 54 (1997); J. Stat. Phys. **88**, 1215 (1997).
[20] T. Gilbert, J. R. Dorfman and P. Gaspard, Phys. Rev. Lett. **85**, 1606 (2000)

[21] P. Gaspard and R. Klages, CHAOS **8**, 409 (1998).
[22] J. Vollmer, T. Tél, and W. Breymann, Phys. Rev. Lett. **79**, 2759 (1997).
[23] J. Vollmer, T. Tél, and W. Breymann, Phys. Rev. E **58**, 1672 (1998).
[24] W. Breymann, T. Tél, and J. Vollmer, CHAOS **8**, 396 (1998).
[25] T. Gilbert, C.D. Ferguson, and J.R. Dorfman, Phys. Rev. E 59, 364 (1999).
[26] T. Gilbert and J.R. Dorfman, J. Stat. Phys. **96**, 225 (1999).
[27] L. Rondoni, T. Tél, and J. Vollmer, Phys. Rev. E **61**, R4679 (2000)
[28] S. Tasaki and P. Gaspard, Theoretical Chemistry Accounts **102**, 385 (1999).
[29] S. Tasaki and P. Gaspard, Entropy production and transport in a conservative multibaker map with energy, to appear in J. Stat. Phys, October 2000.
[30] L. Mátyás, T. Tél and J. Vollmer, Thermoelectric Cross-Effects from Dynamical Systems, Phys. Rev. E **61**, R3295 (2000)
[31] L. Mátyás, T. Tél and J. Vollmer, A MultiBaker map for Thermodynamic Cross-Effects in Dynamical Systems, Phys. Rev. E **62**, 349 (2000)
[32] J. Vollmer, T. Tél, and L. Mátyás, Modeling thermostating, entropy currents and cross effects by dynamical systems, to appear in J. Stat. Phys, October 2000.
[33] L. Rondoni and E.G.D. Cohen: Gibbs Entropy and Irreversible Thermodynamics, `cond-mat/9908367`, to appear in Nonlinearity, November 2000.
[34] I.P. Cornfeld, S.V. Fomin, and Ya.G. Sinai, Ergodic Theory (Springer, Berlin, New York, 1982).
[35] J.P. Eckmann and D. Ruelle, Rev. Mod. Phys. **57**, 617 (1985).
[36] T. Tél, in Directions in Chaos, Vol. 3, ed. Hao Bai Lin (World Scientific, Singapore, 1990) p. 149; in STATPHYS'19, ed. Hao Bai Lin (World Scientific, Singapore, 1996) p. 346.
[37] G. Pianigiani and J.A. Yorke, Trans. Am. Math. Soc. **252**, 351 (1979); T. Tél, Phys. Rev. A 36, 1502 (1987).
[38] H. Kantz and P. Grassberger, Physica D17, 75 (1985).
[39] G. Hsu, E. Ott and C. Grebogi, Phys. Lett. **127 A**, 199 (1988).
[40] L. S. Young, Ergod. Theor. Dyn. Syst. **2**, 109 (1982).
[41] P. Gaspard and X-J. Wang, Physics Reports **235**, 291 (1993).
[42] J.D. Farmer, E. Ott, and J.A. Yorke, Physica D 7, 153 (1983).
[43] P. Grassberger and I. Procaccia, Physica D 13, 34 (1984).
[44] C. Beck and Schlögl, Thermodynamic Formalism (Cambridge Univ. Press, Cambridge, 1993).
[45] F. Reif, Fundamentals of statistical and thermal physics (McGraw-Hill, New York, 1965). For random walks, see Section 1.9.
[46] D.J. Evans, E.G.D. Cohen, G.P. Morriss, Phys. Rev. A 42, 5990 (1990).
[47] W.G. Hoover, A. Posch, and C.G. Hoover, CHAOS **2**, 245 (1992).
[48] W.N. Vance, Phys. Rev. Lett. **69**, 1356 (1992).
[49] D.J. Evans, E.G.D. Cohen, G.P. Morriss, Phys. Rev. Lett. **71**, 2401 (1993).
[50] E.G.D. Cohen, Physica A 213, 293 (1995); Physica A 240, 43 (1997).
[51] G. Gallavotti and E.G.D. Cohen, Phys. Rev. Lett. **74**, 2694 (1995); J. Stat. Phys. **80**, 931 (1995).
[52] L. Rondoni and G.P. Morriss, Phys. Rev. E53, 2143 (1996).
[53] G. Gallavotti, J. Stat. Phys. **85**, 899 (1996); Phys. Rev. Lett. **77**, 4334 (1996).
[54] G. Gallavotti and D. Ruelle, Comm. Math. Phys. **190**, 297 (1997)

[55] W. G. Hoover and H. A. Posch, CHAOS **8**, 366 (1998); Phys. Lett. **246 A**, 247 (1998); W. G. Hoover, J. Chem. Phys. **109**, 4164 (1998).
[56] G. Gallavotti, Physica A 263, 39 (1999).
[57] V.I. Arnold and A. Avez, Ergodic problems of classical mechanics (Benjamin, New York, 1968).
[58] J. Lloyd, L. Rondoni, and G.P. Morriss, Phys. Rev. E **50**, 3461 (1994); G.P. Morriss, C.P. Dettmann and L. Rondoni, Physica A240, 84 (1997); G.P. Morriss and C.P. Dettmann, CHAOS **8**, 321 (1998).
[59] B. Moran, et al., J. Stat. Phys. 48, 709 (1987).
[60] T. Geisel and J. Nierwetberg, Phys. Rev. Lett. **48**, 7 (1982); H. Fujisaka, S. Grossmann, and S. Thomae, Z. Naturf. **40a**, 867 (1986).
[61] R. Klages and J.R. Dorfman, Phys. Rev. Lett. **74**, 387 (1995).
[62] G. Radons, Phys. Rev. Lett. **77**, 4748 (1996); Z. Kaufmann et al., Phys. Rev. Lett. **78**, 4031 (1996).
[63] P. Grassberger, Z. Naturforsch. **43a**, 671 (1988).
[64] W. Feller, An introduction to probability theory and its applications (John Wiley, New York, 1978).
[65] J.L. Lebowitz and H. Spohn, J. Stat. Phys. **19**, 633 (1978); G. Casati et al., Phys. Rev. Lett. **52**, 1861 (1984); D. Szász, A. Krámli, and N. Simányi, J. Stat. Phys. **46**, 303–318 (1987); L.A. Bunimovich and H. Spohn, Comm. Math. Phys. **176**, 661 (1996).
[66] S. Lepri, R. Livi, and A. Politi, Phys. Rev. Lett. **78**, 1896 (1997); D. Alonso et al., Phys. Rev. Lett. **82**, 1859 (1999); C. Wagner, R. Klages, and G. Nicolis, Phys. Rev. E60, 1401 (1999).
[67] D. Landau and E.M. Lifshitz, Electrodynamics of continuous media (London, Pergamon Press, 1960).
[68] N. W. Ashcroft and N. D. Mermin, Solid State Physics, Chapter 16, (Holt, Reinehart and Winston, Saunders College, Philadelphia 1976)
[69] R.C. Tolman, The Principles of Statistical Mechanics (Oxford UP, Oxford, 1938); (reprinted: Dover Publications, New-York, 1979).
[70] D. ter Haar, Rev. Mod. Phys. **27**, 289 (1955)
[71] T.Tél, J. Vollmer, and L. Mátyás, Shear Flow, viscous heating, and entropy balance from dynamical systems, nlin.CD/0009013; and to be published